CANCER

Acetyl-CoA carboxylase 1 controls a lipid droplet–peroxisome axis and is a vulnerability of endocrine-resistant ER$^+$ breast cancer

Marina Bacci[1]†, Nicla Lorito[1]†, Alfredo Smiriglia[1], Angela Subbiani[1], Francesca Bonechi[1], Giuseppina Comito[1], Ludivine Morriset[2], Rania El Botty[2], Matteo Benelli[3], Joanna I. López-Velazco[4], Maria M. Caffarel[4,5], Ander Urruticoechea[4,6], George Sflomos[7], Luca Malorni[3], Michela Corsini[8], Luigi Ippolito[1], Elisa Giannoni[1], Icro Meattini[1,9], Vittoria Matafora[10], Kristina Havas[10], Angela Bachi[10], Paola Chiarugi[1], Elisabetta Marangoni[2], Andrea Morandi[1]*

Targeting aromatase deprives ER$^+$ breast cancers of estrogens and is an effective therapeutic approach for these tumors. However, drug resistance is an unmet clinical need. Lipidomic analysis of long-term estrogen-deprived (LTED) ER$^+$ breast cancer cells, a model of aromatase inhibitor resistance, revealed enhanced intracellular lipid storage. Functional metabolic analysis showed that lipid droplets together with peroxisomes, which we showed to be enriched and active in the LTED cells, controlled redox homeostasis and conferred metabolic adaptability to the resistant tumors. This reprogramming was controlled by acetyl-CoA-carboxylase-1 (ACC1), whose targeting selectively impaired LTED survival. However, the addition of branched- and very long–chain fatty acids reverted ACC1 inhibition, a process that was mediated by peroxisome function and redox homeostasis. The therapeutic relevance of these findings was validated in aromatase inhibitor–treated patient-derived samples. Last, targeting ACC1 reduced tumor growth of resistant patient-derived xenografts, thus identifying a targetable hub to combat the acquisition of estrogen independence in ER$^+$ breast cancers.

INTRODUCTION

Endocrine therapies have revolutionized the clinical management of estrogen receptor–positive (ER$^+$) breast cancer, which accounts for 70% of all breast cancers diagnosed (*1*). Of the endocrine agents available, aromatase inhibitors (AIs), which induce estrogen deprivation, are superior to agents such as tamoxifen and fulvestrant that compete with ER, particularly in postmenopausal women (*2*) and in high-risk premenopausal patients in combination with ovarian suppression (*3*). However, a nonnegligible number of patients relapse during endocrine therapy (*4*). Identifying the potential mechanisms associated with either de novo or acquired resistance is therefore an unmet clinical need (*5*).

Metabolic reprogramming is involved in AI resistance. Of relevance for the current study, we and others have previously reported that ER$^+$ breast cancer cells cultured long-term under estrogen deprivation (LTED), a clinically relevant model of breast cancers that develop resistance to AI treatment, are characterized by enhanced glucose, cholesterol, and selective amino acid metabolic dependency (*6*–*10*). In addition, the balance between de novo fatty acid synthesis (FAS) and lipid breakdown, known as fatty acid beta-oxidation (FAO), is essential for sustaining tumor progression and therapy response (*11*). The rate-limiting step of FAS is catalyzed by acetyl-CoA carboxylase (ACC), which generates malonyl-CoA from acetyl-CoA. Two different isoforms of ACC have been described: acetyl-CoA carboxylase 1 (ACC1) and ACC2, which display similar catalytic activity, although different compartmentalization and functions have been attributed to each. ACC2 is located at the mitochondria surface and generates malonyl-CoA that inhibits the carnitine palmitoyl transferase 1 (CPT-1), hence preventing FA entry into the mitochondria to drive FAO. In contrast, malonyl-CoA generated by cytosolic ACC1 is used by fatty acid synthase (FASN) for de novo FAS in a process that requires NADPH (reduced form of nicotinamide adenine dinucleotide phosphate) (*12*).

On a cellular level, lipid droplets (LDs) have a major role in balancing de novo lipogenesis and FAO. It is now established that LDs are not solely storage hubs for neutral lipids but are dynamic organelles with essential biological and metabolic functions (*13*). Crucially, in nonlipogenic tissues, LDs accumulate when cells are under stress conditions, and increased LDs were reported in various neoplastic processes (*14*–*16*). Moreover, LDs can function as a link between mitochondria and peroxisomes, providing an intracellular network controlling lipid metabolism (*17*). In mammals, most FAO occurs in mitochondria, but peroxisomes are essential for the oxidation of very long–chain fatty acids (VLCFAs) and branched-chain fatty acids (BCFAs). Recent findings indicate that LDs and peroxisomes cooperate in controlling lipolysis and reactive oxygen species (ROS) handling during non-alcoholic fatty liver disease progression

[1]Department of Experimental and Clinical Biomedical Sciences, University of Florence, Viale Morgagni 50, 50134 Florence, Italy. [2]Laboratory of Preclinical Investigation, Translational Research Department, Institut Curie, PSL University, 26 rue d'Ulm, 75005 Paris, France. [3]Department of Medical Oncology, Azienda USL Toscana Centro, Hospital of Prato, Via Suor Niccolina Infermiera 20, 59100 Prato, Italy. [4]Biodonostia Health Research Institute, Paseo Dr Begiristain s/n, 20014 San Sebastian, Spain. [5]Ikerbasque, Basque Foundation for Science, Plaza Euskadi 5, 48009 Bilbao, Spain. [6]Gipuzkoa Cancer Unit, OSI Donostialdea–Onkologikoa Foundation, Paseo Dr Begiristain 121, 20014 San Sebastian, Spain. [7]Swiss Institute for Experimental Cancer Research, School of Life Sciences, Ecole Polytechnique Fédérale de Lausanne, CH-1015 Lausanne, Switzerland. [8]Department of Molecular and Translational Medicine, University of Brescia, Via Branze 39, 25123 Brescia, Italy. [9]Radiation Oncology Unit, Oncology Department, Azienda Ospedaliero Universitaria Careggi, Largo Brambilla 3, 50134 Florence, Italy. [10]IFOM ETS–AIRC Institute of Molecular Oncology, Via Adamello 16, 20139 Milan, Italy.
*Corresponding author. Email: andrea.morandi@unifi.it
†These authors contributed equally to this work.

(*18*). However, little is known about the role of peroxisomes in controlling metabolic deregulation during cancer progression (*19*).

In particular, a role for peroxisome- and LD-dependent metabolic reprogramming and the implication in response and resistance to therapy in breast cancer have yet to be explored. Here, we show that targeting ACC1 restrains the lipid metabolic plasticity of AI-resistant breast cancers altering the cross-talk between LDs and peroxisomes, thus validating a potential metabolic vulnerability of clinical and prognostic relevance in endocrine resistance.

RESULTS

Estrogen-independent ER$^+$ breast cancer cells show NF-κB–dependent aberrant lipid metabolism that enhances intracellular lipid deposition

LTED cells are derived from parental cells by culturing in the absence of estradiol (E2) for 6 to 12 months. This is an established model to study AI resistance (Fig. 1A) (*7*, *20*). Aberrant lipid metabolism is a trait of resistant cancers. Enrichment analysis of parental ER$^+$ MCF7 cells [also referred as wild-type (WT)] and LTED counterparts suggested a potential role of adipogenesis (14 gene sets; *P*-adj < 0.05) and lipid metabolism (90 gene sets; *P*-adj < 0.05) in AI resistance (data file S1). To address the potential metabolic differences related to lipid metabolism in endocrine therapy resistance, we subjected to lipidomic analysis an isogenic model in which parental ER$^+$ MCF7 cells were compared with LTED derivatives. Cell lysis was performed on three independent replicates, and total lipids were extracted and subjected to mass spectrometry analysis [nano-liquid chromatography–electrospray ionization–tandem mass spectrometry (nLC-MS/MS)] (*21*). Lipidomic analysis identified 2109 lipid species (data file S2). Principal components analysis (PCA) of the identified entities showed a separation between the samples derived from either parental or LTED cells (Fig. 1B, left). Of the lipid species identified, glycerolipids are those with a major contribution to the differential clustering between parental and LTED samples (fig. S1A). LipidSig (*22*) analysis showed that LTED cells are enriched in triglycerides, glycerophospholipids, and cholesteryl esters compared with parental cells (fig. S1B). LIpid ONtology (LION) enrichment analysis (*23*) revealed lipid storage, LDs, and triacylglycerols as the most significant enriched lipidomic terms (Fig. 1B, right). Moreover, enrichment analysis of the transcriptomic data [GOCC_LIPID_DROPLET (*P*-adj = 0.0001) and GOBP_LIPID_STORAGE (*P*-adj = 0.0005); data file S1] supported the lipidomic data. To determine whether the enrichment analyses were paralleled by a change in the intracellular lipid deposition and whether this could be a feature of cells modeling AI resistance, we stained a panel of isogenic LTED cell lines with the fluorescent neutral lipid dye BODIPY$^{493/503}$, which is retained in LDs. Confocal image quantification showed that LTED cells were enriched in LD content (Fig. 1C). Moreover, LTED cells expressed higher amounts of Perilipin (PLIN) family proteins, namely, PLIN4 and PLIN5, that were interspersed in the phospholipid layer of LDs (fig. S1C) and enhanced in LD-high expressing cells (*13*).

To examine whether the increase in LD content is a consequence of enhanced dependency on de novo lipogenesis, cells were cultured in media supplemented with radiolabeled ^{14}C-glucose. Labeling of intracellular ^{14}C-lipids revealed an increase in LTED de novo lipogenesis compared with parental cells (Fig. 1D). The increased LDs of LTED cells were independent of the charcoal-dextran stripped serum (DCC) used for LTED cell culture (fig. S1D), which is exclusively deprived of free cholesterol as previously shown by LC-MS/MS analysis (*24*). In line with an enrichment in glucose-dependent lipid content in the LTED cells, quantitative reverse transcription polymerase chain reaction (qRT-PCR) and Western blot analyses showed increased abundance of adenosine triphosphate (ATP) citrate lyase (ACLY) and FASN together with activation of ACC1 (revealed by its decreased phosphorylation; Fig. 1, E and F) but not of ACC2 (fig. S1E), an enzymatic asset associated with de novo lipogenesis. Because the activation of transcription factor nuclear factor κB (NF-κB) has been associated with endocrine therapy resistance (*25*) and it is established that NF-κB controls lipid metabolism, at least in the cancer context (*26*), we postulated that the lipid metabolic reprogramming of the LTED cells could be NF-κB dependent (26 NF-κB–related gene sets are associated with LTED transcriptomic profile; *P*-adj < 0.05; table S1). The administration of the selective IκB kinase inhibitor [5-(p-fluorophenyl)-2-ureido]thiophene-3-carboxamide (TPCA-1), known to impair NF-κB activation, had a higher effect in reducing cell survival in the LTED than the WT MCF7 cells (Fig. 1G). Crucially, TPCA-1 administration reduced ACC1 activation (indicated by increased phosphorylation) and ACLY abundance (Fig. 1H), a reprogramming that inhibited de novo FAS, as revealed by ^{14}C-tracing experiments (Fig. 1I and fig. S1F) and LD accumulation (Fig. 1J and fig. S1G) in LTED cells.

LD-dependent lipid mobilization sustains estrogen independence

It has been reported that a subset of breast cancer cells responsible for tumor recurrence show concomitant enhanced lipogenesis and oxidative capacity (*16*). Our previous gene set enrichment analysis revealed a positive association with the gene set FATTY_ACID_OXIDATION [M14568, normalized enrichment score (NES): 1.61; *P* = 0.018 (*7*)] and the LTED transcriptomic profile, suggesting potential enhancement of FAO in LTED cells. Lipid-dependent oxidative capacity was assessed by real-time measurement of the oxygen consumption rate (OCR) using Seahorse analysis. A mitochondrial stress test revealed that basal and maximal respiration were significantly higher in LTED than in WT cells (Fig. 2A). Blocking lipid entry into mitochondria using the CPT-1 inhibitor etomoxir decreased the respiratory capacity of WT cells. In contrast, LTED cells were marginally affected (Fig. 2A and fig. S2A). The Seahorse mito fuel flex test, which revealed the relative contribution of glucose, glutamine, and long-chain fatty acid (LCFA) oxidation to oxidative metabolism under metabolic constriction, confirmed the enhanced metabolic flexibility of LTED cells (Fig. 2B). Because LDs have a prominent role during nutrient starvation (*27*), we cultured WT and LTED cells in low glucose and low serum conditions (limited medium). Three-day limited culturing conditions had a major impact on WT cell survival with only a minimal effect in LTED cells (Fig. 2C). Upon limited conditions, etomoxir had a substantial effect in reducing OCR as revealed by Seahorse analysis (Fig. 2D and fig. S2B) and affected LTED cell survival (Fig. 2E). Therefore, the lipid-dependent oxidative capacity of LTED cells could be fueled by internal lipid depots. Limited culture conditions rapidly reduced LD content within LTED cells but increased LD content in WT cells (Fig. 2F), a phenomenon that has been associated with nutrient stress conditions (*28*). Adipose triglyceride lipase (ATGL) mediates lipolysis of triacylglycerols stored in LD, and its expression was higher in LTED compared with parental cells (fig. S2C). Confocal

analysis and subsequent quantification of BODIPY$^{493/503}$ showed that ATGL inhibition (atglistatin, ATGLi) abrogated the LD consumption induced by limited culture conditions (Fig. 2F). On the basis of this observation, a longer ATGLi treatment (72 hours) in combination with nutrient starvation reduced LTED cell survival (Fig. 2G), suggesting that LD mobilization may sustain the AI desensitization properties of LTED cells. ATGLi impaired the oxidative capacity of LTED cells during limited culturing conditions, as shown by OCR impairment (Fig. 2, H and I, and fig. S2, D and E), demonstrating a key role of LD-dependent lipid catabolism in sustaining the energetic capacity of LTED cells.

PLIN2 expression after neoadjuvant endocrine therapy predicts endocrine therapy resistance

To validate whether the LD presence is associated with anti-estrogen therapy response in the clinic, we examined a cohort of patients with ER$^+$ breast cancer who underwent neoadjuvant endocrine therapy (NET) in the preoperative setting (Fig. 3A) (*29*). In such

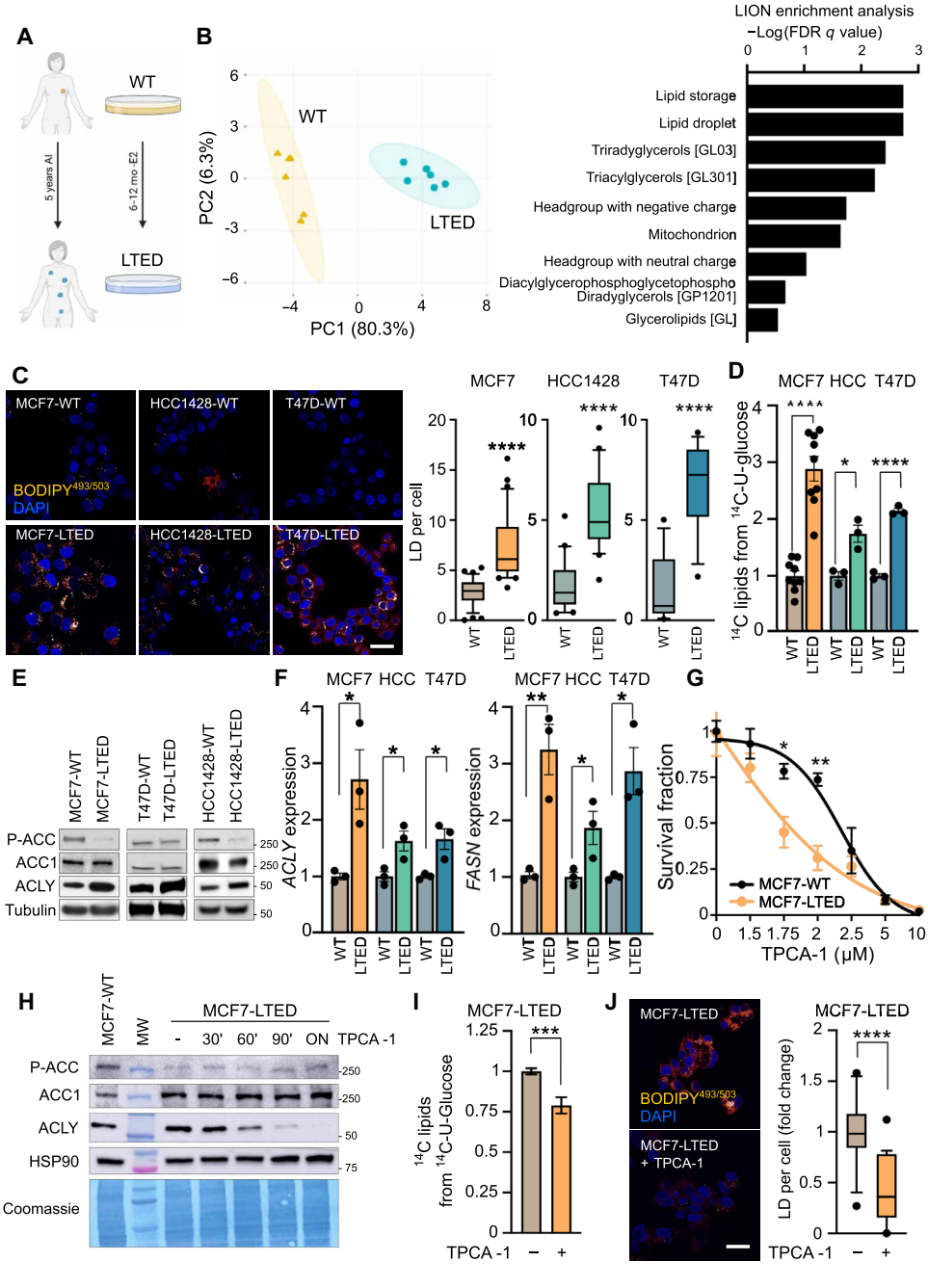

Fig. 1. LTED cells show enhanced LDs sustained by de novo lipogenesis. (**A**) Schematic representation of the in vitro LTED model, which mimics development of resistance to AIs in patients. (**B**) PCA of sensitive and resistant MCF7 lipidomic profiles (left). LION enrichment analysis and correlation between LTED profile and LD-related signatures (right). (**C**) Confocal analysis of parental and LTED cells. Representative BODIPY$^{493/503}$-stained cells are shown [orange/yellow: LD; blue: 4′,6-diamidino-2-phenylindole (DAPI), nuclei] with quantification of BODIPY spots per cell. Scale bar, 10 μm. $n = 3$ biological replicates in ≥3 technical replicates. (**D**) LTED and MCF7 breast cancer cells were cultured overnight in medium containing ^{14}C glucose. Lipids were extracted and radioactive signal was measured to monitor ^{14}C glucose incorporation into lipids. Values were normalized by protein content. (**E**) Western blot analysis of total protein lysate from MCF7, T47D, and HCC1428 parental cells and their corresponding LTED derivatives using indicated antibodies. (**F**) LTED-derived and parental cells analyzed by qRT-PCR analysis. Fold enrichment is relative to parental cells. (**G**) MCF7-LTED and parental cells were treated with increasing TPCA-1 concentrations for 3 days and subjected to crystal violet survival assay. $n = 3$ biological replicates. (**H**) Total protein lysates from MCF7 and MCF7-LTED cells treated with 1.75 μM TPCA-1 for indicated times were subjected to Western blot analysis with indicated antibodies. (**I**) WT and LTED MCF7 cells were treated with 1.75 μM TPCA1 for 24 hours and cultured overnight in medium containing ^{14}C glucose. Lipids were extracted and to measure ^{14}C glucose incorporation into lipids. Values were normalized by protein content. $n = 4$ biological replicates in three technical replicates. (**J**) MCF7-LTED cells were treated with 1.75 μM TPCA1 for 24 hours and subjected to confocal analysis (orange yellow: LD; blue: DAPI, nuclei). LDs were quantified. Representative images shown. Scale bar, 10 μm. $n = 3$ biological replicates; each point is a technical replicate. Data are mean ± SEM. (D, F, and I) Student's *t* test. (G) Two-way ANOVA, Bonferroni-corrected. (C and J) Boxplot indicates 10th and 90th percentiles (whiskers), 25th and 75th quartiles (box), and mean. (C and J), Mann-Whitney test. $^*P < 0.05$; $^{**}P < 0.01$; $^{***}P < 0.001$; $^{****}P < 0.0001$. FDR, false discovery rate; MW, molecular weight.

studies, low Ki67 proliferation index and preoperative prognostic index (PEPI) score after NET are associated with a positive long-term prognosis (*30*, *31*). We previously showed that PLIN2 staining can be used as a proxy of the LD presence within cancer-derived specimens (*15*), and we stained the breast sample cores of the tissue microarrays (TMAs) accordingly (Fig. 3B). Ki67 score after NET (Fig. 3, C and D) and modified PEPI score (Fig. 3, E and F) were higher in patients with higher PLIN2 scores, hence suggesting that PLIN2, and therefore the LD presence, could hold predictive endocrine therapy value.

ACC1 targeting resensitizes LTED cells to estrogen deprivation

To identify potential metabolic vulnerabilities linked to the lipid metabolic reprogramming displayed by LTED cells, we comparatively assessed the cell survival changes induced in WT and LTED MCF7 cells exposed to agents that target lipid-related metabolic pathways. Targeting ACLY (MEDICA16 and SB204990), FASN (TVB3166 and C75), FAO (etomoxir), and the mevalonate pathway (simvastatin and zoledronic acid) showed no significant differences between WT and LTED cells. However, ACC1 targeting using the allosteric inhibitor TOFA

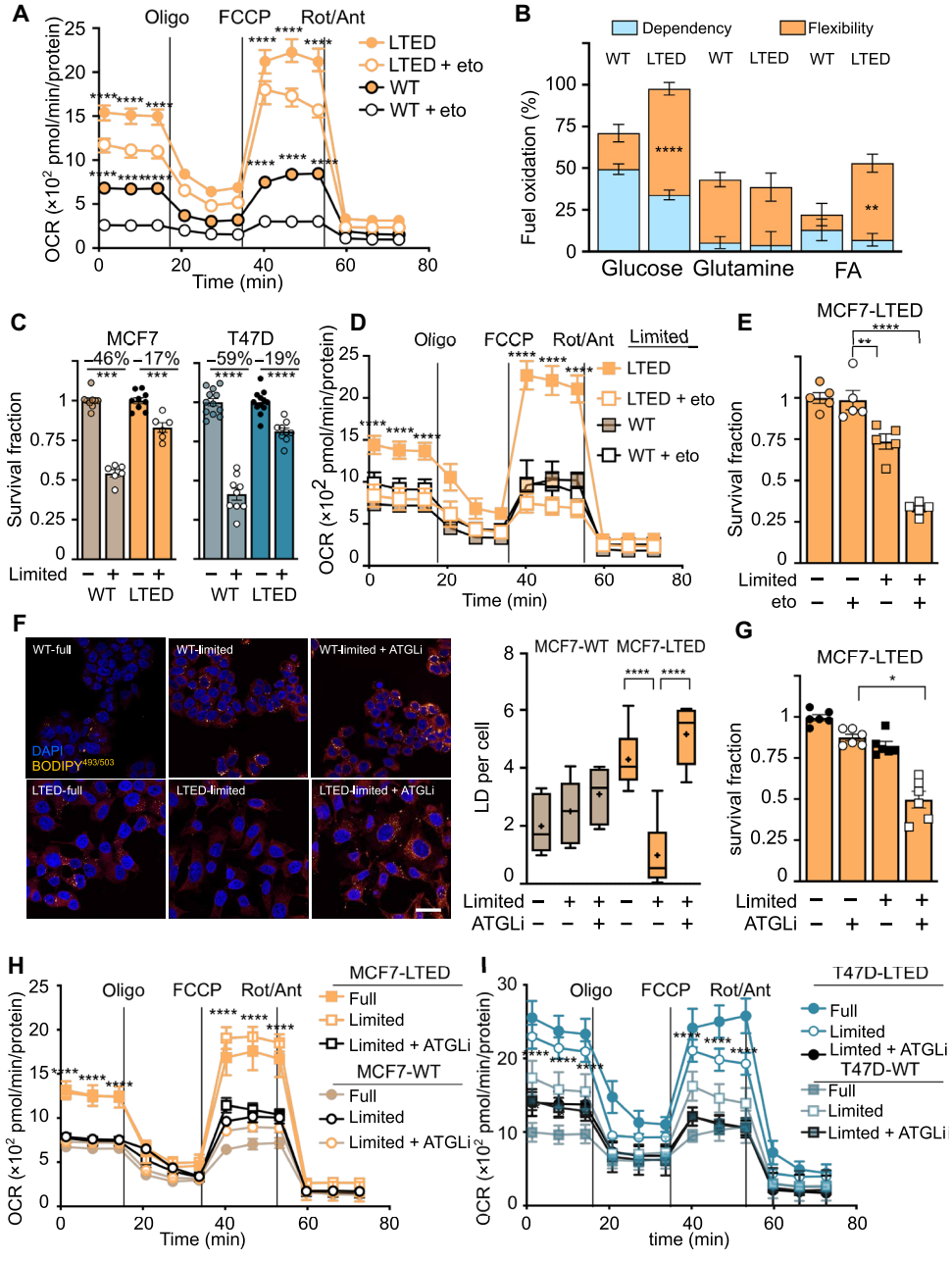

Fig. 2. LD-dependent lipid mobilization sustains resistance to estrogen deprivation. (**A**) Seahorse XFe96 Mito Stress Test on WT parental and MCF7-LTED cells treated with 40 μM etomoxir (eto) for 1 hour in standard conditions (full medium). OCR was calculated in real time after administration of ATP synthase inhibitor oligomycin, proton uncoupler carbonilcyanide p-triflouromethoxyphenylhydrazone (FCCP), and respiratory complex I inhibitor rotenone together with respiratory complex III inhibitor antimycin A (Rot/Ant). $n \geq 3$ biological replicates. LTED versus LTED + eto; WT versus WT + eto; two-way ANOVA, Tukey-corrected. (**B**) Seahorse XFe96 Mito Fuel Flex Test was performed on parental and MCF7-LTED cells, and fuel oxidation was calculated and normalized by protein content. $n = 3$ biological replicates in ≥5 technical replicates. Student's *t* test. (**C**) WT and LTED cells were grown either in standard conditions or in limited medium for 72 hours before assaying cell viability. Data are fold change survival fraction of LTED versus WT cells. Each dot is a biological replicate. Mann-Whitney test for MCF7-WT and Student's *t* test for other cell lines. (**D**) Seahorse XFe96 Mito Stress Test was performed on MCF7-WT and MCF7-LTED cells cultured under nutrient deprivation in the presence or absence of 40 μM eto for 1 hour. OCR was calculated in real-time and normalized by protein content. $n = 5$ biological replicates. LTED versus LTED + eto; two-way ANOVA, Tukey-corrected. (**E**) MCF7-LTED cells were grown either in standard conditions or in limited medium for 72 hours with or without 40 μM eto before subjecting them to cell viability assay. $n = 5$ biological replicates. One-way ANOVA; Dunnett-corrected. (**F** to **I**) LTED cell derivatives and parental cells were grown in either full or limited medium with or without 25 μM ATGLi for (F) 24 hours and LD BODIPY$^{493/503}$-stained [(orange/yellow), DAPI, nuclei (blue); representative pictures and quantification of BODIPY spots per cell are shown; plot indicates 10th and 90th percentiles (whiskers), 25th and 75th quartiles (box), mean (line), and median (cross). $n = 3$ biological replicates, one-way ANOVA, Tukey-corrected; scale bar, 10 μm], or (G) 72 hours and subjected to cell viability assay (data are fold change survival fraction of LTED versus WT cells. $n = 6$ biological replicates. One-way ANOVA, Kruskal-Wallis Dunn-corrected), or 1 hour for parental and LTED derivatives (H) MCF7 and (I) T47D cell lines. OCR from Mito Stress Test analysis was reported ($n = 3$ biological replicates in ≥2 technical replicates, LTED limited versus LTED limited + ATGLi; two-way ANOVA, Tukey-corrected). (C to E and G to I) Data are mean ± SEM. * $P < 0.05$; ** $P < 0.01$; *** $P < 0.001$; **** $P < 0.0001$.

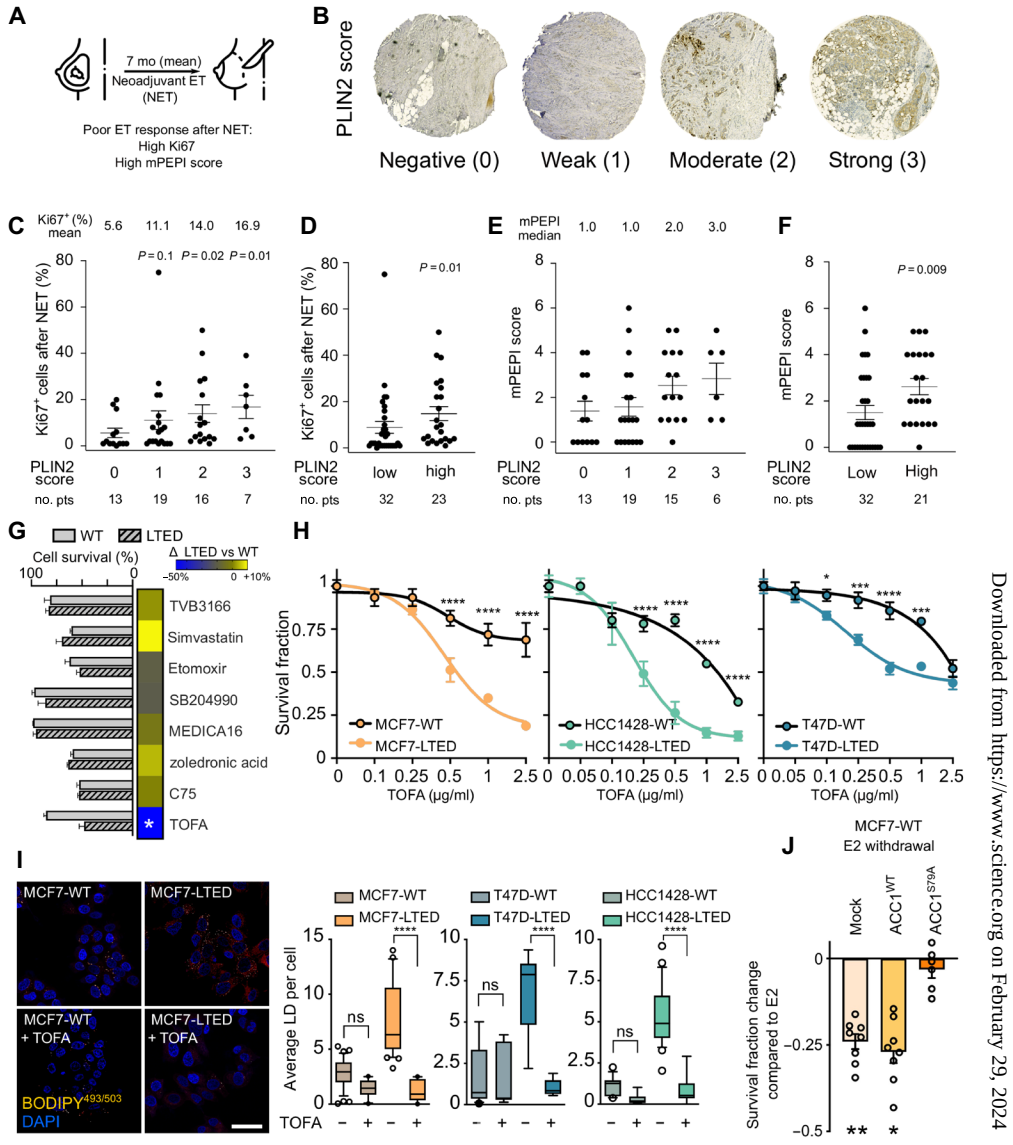

Fig. 3. PLIN2 correlates with worse prognosis in endocrine-treated breast cancer, and targeting ACC1 reduces LDs and survival of estrogen-deprived LTED cells. (**A**) Schematic of the NET study from which surgical specimens were included in TMAs and subjected to PLIN2 IHC staining. (**B**) Representative IHC staining for PLIN2 in the TMA cores. Magnification, ×40. (**C** to **F**) Percentage of Ki67 cells (C and D) and modified PEPI score (E and F) at surgery (after NET) in the patients with breast cancer subdivided by PLIN2 IHC score (C and E) or by low (scores, 0 + 1) and high (scores, 2 + 3) PLIN2 expression (D and F). Mann Whitney test (C to F). (**G**) MCF7-LTED and parental cells were treated with a series of drugs targeting lipogenic enzymes and assayed for cell viability. Data are mean ± SEM. $n = 3$ biological replicates. Student's *t* test. (**H**) Three-day dose-response curves of TOFA analyzed by crystal violet assays in all the LTED derivatives. Data are mean ± SEM. $n = 3$ biological replicates in ≥1 technical replicate; two-way ANOVA, Tukey-corrected. (**I**) LTED and parental cells were treated with TOFA (0.5 μg/ml) for 16 hours and subjected to confocal analysis (LDs = orange/yellow; nuclei = blue; scale bar, 10 μm). Quantification of BODIPY$^{493/503}$ spots per cell was reported for all cell lines. Plots indicate 10 and 90 percentiles (whiskers), 25 and 75 quartiles (box), and mean (line). $n = 3$ biological replicates in ≥3 technical replicates; one-way ANOVA, Kruskal-Wallis, Dunn-corrected. (**J**) MCF7-WT cells expressing constitutively active ACC1 (ACC1^{S79A}) or wild-type form (ACC1^{WT}) were grown for 5 days in DCC medium with or without 1 nM E2 before assaying cell viability. Mock indicates cells only treated with transfection reagent. Data are fold change survival fraction of no E2 versus E2-cultured cells. $n = 3$ biological replicates in ≥2 technical replicates. Data are mean ± SEM and were compared with the corresponding E2-cultured cells using the Student's *t* test. $^*P < 0.05$; $^{**}P < 0.01$; $^{***}P < 0.001$; $^{****}P < 0.0001$.

(5-tetradecyloxy-2-furoic acid) selectively impaired LTED cell survival (Fig. 3G). This selective effect was confirmed in a 3-day dose response scheduled treatment in a panel of isogenic ER$^+$ LTED cells (Fig. 3H). On a metabolic functional level, 16-hour TOFA administration was sufficient to impair the catabolic ability of LTED cells, as revealed by OCR and oxygen consumption real-time monitoring using Seahorse analysis and Oroboros oxygraph-2K high-resolution respirometer (fig. S3).

Because of the crucial role that LDs have in sustaining AI resistance, we investigated whether ACC targeting could affect LD content in LTED cells before inhibiting cell survival. Sixteen hours of TOFA administration eliminated intracellular lipid depots, as shown by confocal analysis of BODIPY$^{493/503}$ staining in LTED cells (Fig. 3I and fig. S4A) and impaired glucose-dependent de novo FAS (fig. S4B). Genomic approaches and the administration of a second ACC inhibitor [ND646 (*32*)] were used to exclude off-target effects exerted by TOFA. ACC1 silencing using multiple siRNAs (fig. S4, C to G) and dose-dependent administration of ND646 (fig. S4, H and I) reduced LTED cell survival (fig S4, C, D, and H), LD content (fig. S4, C, D, F, and I), and de novo lipid synthesis (fig. S4G). ND646 inhibited both ACC1 and ACC2 and therefore precluded the ability of ACC2 to compensate for ACC1 inhibition. Moreover, ACC2 was phosphorylated in the LTED cells, indicating that its action is negligible in our model (fig. S1E). Because ACC1 inhibition impaired the metabolic reprogramming of LTED cells and subsequent cell survival, we analyzed the effects of ACC1 overexpression when parental cells were subjected to estrogen withdrawal (Fig. 3J and fig. S4J). Ectopic expression of the constitutive active form of ACC1 [ACC1^{S79A} (*33*)] rendered MCF7-WT cells insensitive to estrogen withdrawal, whereas stable expression of the WT form of ACC1 (ACC1^{WT}) did not (Fig. 3J), suggesting that ACC1 activation is involved in the acquisition of resistance to estrogen deprivation.

LTED cells show enhanced lipid upload capacity and metabolic plasticity

Because impairing acetyl-CoA elongation had a modest effect in reducing cell viability in both parental and LTED cells (Fig. 3G), we

investigated whether targeting FASN in limited conditions could enhance such impairment, because we concomitantly impeded de novo lipogenesis and consumed the LD internal reserve. When FASN inhibitor TVB3166 was administrated under limited conditions, it had a significant effect in reducing cell viability in both parental and LTED cells. However, the addition of palmitate reverted the inhibitory effect of TVB3166 exclusively in LTED cells, suggesting that LTED cells could use external palmitate, thus bypassing FASN impairment (Fig. 4A).

The fatty acid transporter *CD36* was up-regulated in LTED cells according to interrogation of our previously published transcriptomic analysis (*7*) and validation by qRT-PCR (Fig. 4B). Functionally, LTED cells internalized more exogenous palmitate as shown by radiolabeled ^{14}C-palmitate upload assay (Fig. 4C) and by monitoring cellular ability to upload fluorescent labeled palmitate (BODIPY-FL-C_{16}) using confocal microscopy and cytofluorimetric analysis (Fig. 4, D and E).

ACC1 targeting alters the LD-peroxisome axis and subsequent redox balance in LTED cells

LDs have a fundamental role in buffering intracellular ROS and diminishing lipid peroxidation, which is toxic to cells (*34*). LTED cells showed higher ROS content than WT cells (Fig. 5, A and B, and fig. S5A), and treatment with the antioxidant N-acetylcysteine decreased LD content in resistant cells (fig. S5B), indicating that a balance between oxidative state and lipid metabolism exists. Because impairing ACC1 in the LTED cells altered lipid metabolism and LD content, we postulated that TOFA could alter redox homeostasis. TOFA administration enhanced ROS in the LTED cells, as monitored by ROS-measuring fluorescent probes (Fig. 5, A and B, and fig. S5C). The increased ROS were paralleled by enhanced lipid peroxidation as indicated by production of the end product of FA peroxidation malondialdehyde (Fig. 5C) and by confocal analysis of oxidized lipids using BODIPY$^{581/591}$ C11 fluorescent probe (Fig. 5D). Because lipid peroxidation products have been associated with iron-dependent cell death (ferroptosis) (*35*), we targeted ACC1 in the presence of the radical-trapping antioxidant ferrostatin-1. No change in cell viability or lipid peroxidation was observed when TOFA and ferrostatin-1 were administrated concomitantly (fig. S5, D and E), suggesting that the toxicity exerted by ACC1 inhibition is ferroptosis independent.

Because LTED cells showed elevated oxidative phosphorylation capacity (Fig. 2A), we hypothesized that mitochondria (electron transport chains) may be the source of enhanced ROS. However, staining of the mitochondrial-derived ROS using the fluorescent probe MitoSOX revealed no difference between parental and LTED cells, either in the presence or absence of TOFA (Fig. 5E). We therefore extrapolated the OCR data from the Seahorse analysis and found that LTED cells showed enhanced nonmitochondrial OCR compared with parental cells (Fig. 5F), which we validated by measuring the residual oxygen consumption using the Oroboros oxygraph-2K high-resolution respirometer (fig. S6A). The oxidation of VLCFAs and BCFAs initiates in the peroxisome and is a process that depends on acyl-CoA oxidase 1 (ACOX1) and produces H_2O_2. ROS abundances are then buffered within the peroxisome matrix by the catalase (CAT) enzyme, which neutralizes H_2O_2 into H_2O and O_2 (*36*). LTED cells showed enhanced content of peroxisomes as detected by confocal analysis (Fig. 5G) and quantified by FACS analysis (Fig. 5H) using a green fluorescent protein (GFP)–labeled fusion construct of a peroxisomal C-terminal targeting sequence. Moreover, the enhanced peroxisome content was paralleled by increased expression of the peroxisome functional players *CAT* and *ACOX1* (Fig. 5I). This enhanced peroxisome dependence was corroborated at the transcript level given that the HALLMARK_PEROXISOME gene set positively associated with the LTED transcriptional profile (*P*-adj = 0.0023; data file S1). The clinical relevance of the peroxisome signature was validated in two large retrospective cohorts of patients with breast cancer [Molecular Taxonomy of Breast Cancer International Consortium (METABRIC) (*37*) and the Cancer Genome Atlas (TCGA)] in which the

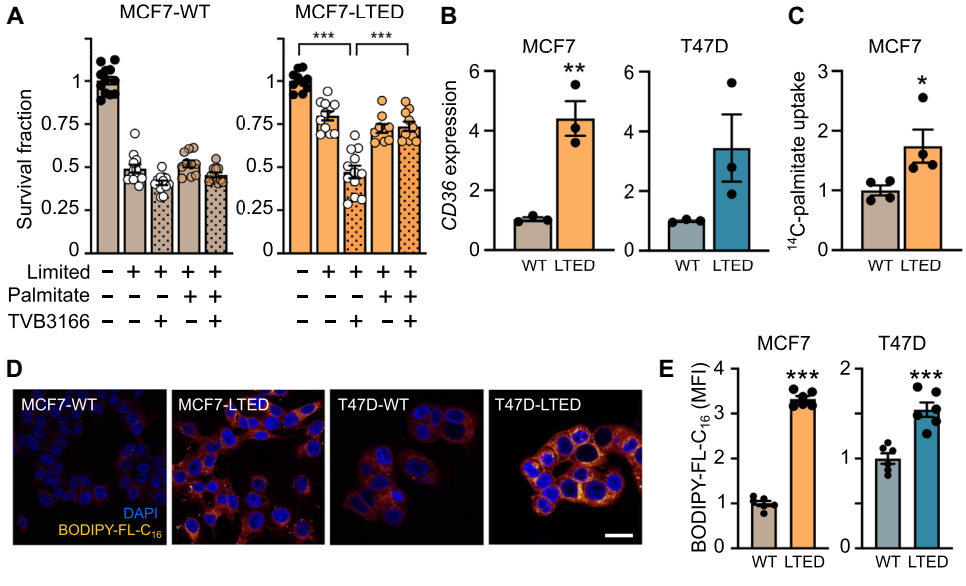

Fig. 4. LTED cells show enhanced lipid upload capacity and metabolic plasticity. (**A**) MCF7 WT and LTED cells cultured in limited condition were treated with 200 μM TVB3166 and 10 μM palmitate for 72 hours and assayed for cell viability. Data are fold change survival fraction compared to cells grown in routine culture conditions and shown as mean ± SEM. $n = 3$ biological replicates in ≥3 technical replicates. One-way ANOVA, Dunnett-corrected. (**B**) MCF7 and T47D parental and their counterpart LTED cells were subjected to qRT-PCR for *CD36* analysis. Fold change relative expression is shown using parental cells as comparator. Each dot represents a biological replicate. (**C**) ^{14}C-palmitate uptake was measured in LTED-derived and parental MCF7 cells. Relative upload capacity is shown using parental cells as comparator. Each dot represents a biological replicate. (**D**) Sensitive and resistant cells were incubated with 100 nM BODIPY-C_{16}, and palmitate uptake was observed as orange/yellow fluorescence. DAPI counterstain shows nuclei (blue). Representative images are shown. Scale bar, 10 μm. (**E**) Parental and their derivative LTED cells were subjected to cytofluorimetric analysis. FACS analysis of the mean fluorescence intensity (MFI) of the populations positive for BODIPY FL-C16 was reported. Each dot represents a biological replicate. (B, C, and E) Data are mean ± SEM; Student's *t* test. **P* < 0.05; ***P* < 0.01; ****P* < 0.001.

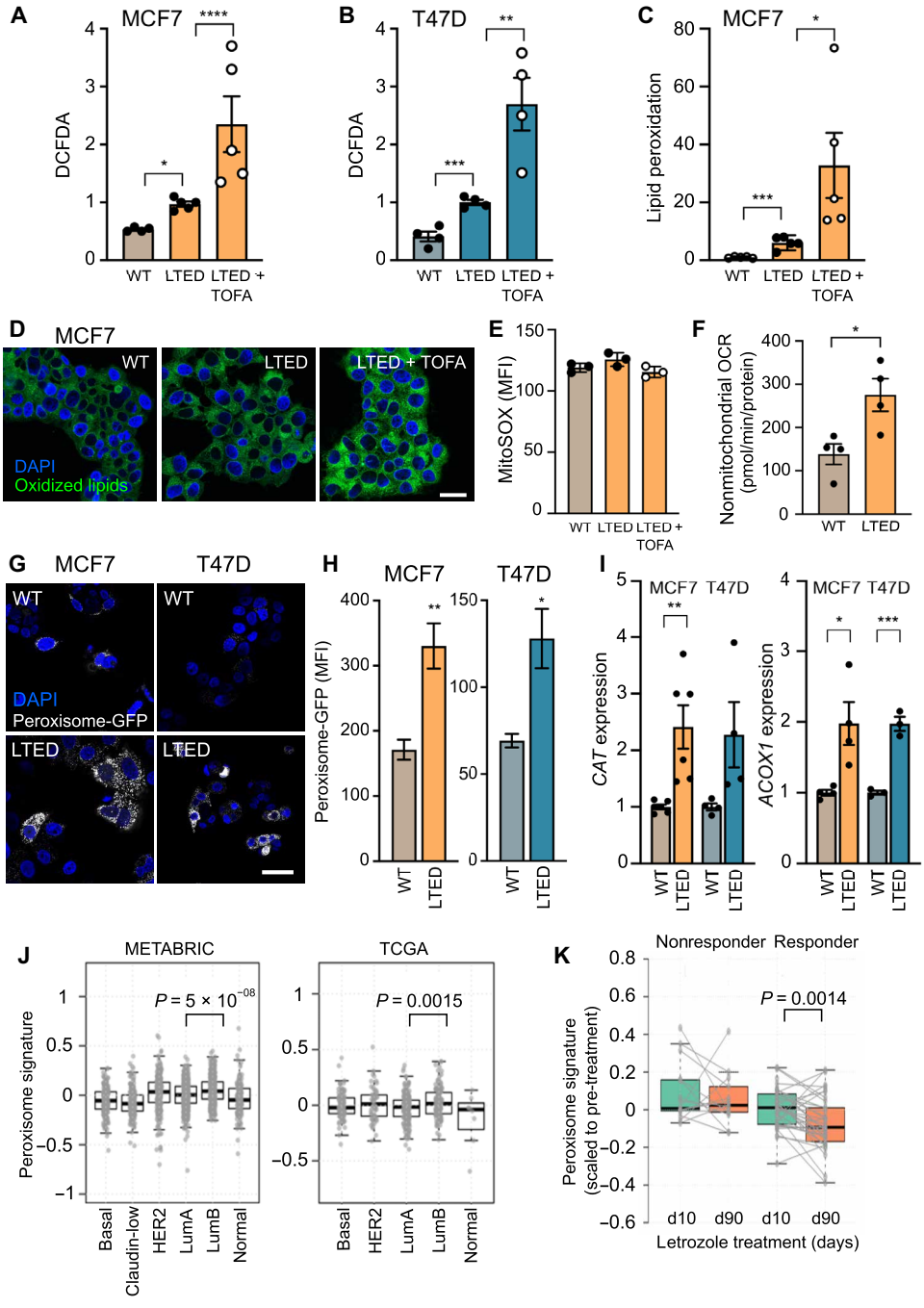

Fig. 5. ACC1 targeting alters the LD-peroxisome axis and subsequent redox balance of LTED cells. (**A** and **B**) Intracellular ROS were measured by 2′,7′-dichlorofluorescin diacetate (DCFDA) staining in MCF7 (A) and T47D (B) WT and LTED cells treated with TOFA (0.5 μg/ml) for 72 hours. Parental cells were used as comparator. Each dot represents a biological replicate. Student's *t* test. (**C** and **D**) Lipid peroxidation was evaluated by measuring the malondialdehyde (MDA) intracellular accumulation (C) and fluorescence intensity of BODIPY$^{581/591}$ C11 (D) in MCF7 parental and LTED cells treated with TOFA (0.5 μg/ml) for 48 hours. Representative confocal images are shown (oxidized lipids, green; blue: DAPI, nuclei; scale bar, 10 μm). Each dot represents a biological replicate. Student's *t* test. (**E**) Mitochondrial ROS were measured using the fluorescent probe MitoSOX in MCF7-WT and MCF7-LTED cells treated with TOFA (0.5 μg/ml) for 72 hours. Parental cells were used as comparator. Each dot represents a biological replicate. One-way ANOVA; Dunnett-corrected. (**F**) Nonmitochondrial OCR measurement was extrapolated from the Seahorse Mito Stress Test analysis and compared between parental and LTED MCF7 cells. Each dot represents a biological replicate. Student's *t* test. (**G** and **H**) Parental and LTED MCF7 and T47D cells were subjected to peroxisome content confocal and cytofluorimetric analysis. Representative pictures (G) of CellLight Peroxisome-GFP stained cells are shown (gray/white: peroxisomes; blue: DAPI, nuclei). Scale bar, 10 μm. FACS analysis of the MFI of the populations positive for the GFP-peroxisome construct was reported (H). Student's *t* test for MCF7 versus MCF7-LTED and Mann-Whitney test for T47D versus T47D-LTED. (**I**) Analysis of peroxisomal activity in MCF7 and T47D-LTED cells compared with their parental counterpart was performed by qRT-PCR for *ACOX1* and *CAT*. Fold relative enrichment is shown using the parental cells as comparator. Each dot represents a biological replicate. Student's *t* test. (**J**) Analysis of publicly available clinical data (METABRIC and TCGA) derived from patients with ER$^+$ breast cancer showed that peroxisome signature correlates with luminal B phenotype. (**K**) Changes in peroxisome signature scaled to pretreatment in 52 paired ER$^+$ breast cancer samples pre– and post–2-week AI treatment (letrozole) among responder patients ($n = 37$) and nonresponders ($n = 15$). (A to I) Data are mean ± SEM. *$P < 0.05$; **$P < 0.01$; ***$P < 0.001$; ****$P < 0.0001$.

peroxisome signature was significantly higher in the luminal B than in the luminal A subtype (Fig. 5J). Further, subtyping analysis of the peroxisome gene set revealed that the difference was independent of HER2 status (fig. S6B). Within ER$^+$ breast cancers, luminal B tumors are characterized by increased therapy resistance, relapse, and poorer prognosis compared with luminal A (*38*), suggesting that peroxisome signature can be associated with a clinically relevant molecular subtype. To investigate a potential predictive value of the peroxisome signature in response and resistance to AI, we retrieved the publicly available gene expression data from 52 ER$^+$ breast cancer patient specimens taken before and after 10 days and 90 days of neoadjuvant letrozole treatment (*39*). Patients were divided into responders and nonresponders, defined by a >50% and a <50% reduction, respectively, in tumor volume after a further 3 months of letrozole treatment. The peroxisome signature was significantly (paired Wilcoxon test, $P = 0.0014$) decreased in the responder cohort after 90 days of letrozole treatment, suggesting that a decrease in this transcriptional profile could be associated with therapy response (Fig. 5K). No significant changes were reported in the nonresponder cohort, suggesting a potential link with letrozole resistance. Particularly, because the significant differences between responder and nonresponder patients emerged after 90 days of therapy, this

could suggest that the peroxisome contribution to therapy response might become relevant after therapy exposure and therefore be involved in the acquired rather than in de novo endocrine resistance.

ACC1 activity is dispensable for LTED cells in the presence of exogenous complex FA

VLCFA, LCFA, and BCFA synthesis depends on malonyl-CoA generated by ACC1 and NADPH as reducing agent (*40*). LTED cells showed increased FAS from radioactive palmitate (fig. S6C), suggesting that exogenous palmitate could be used by LTED cells to synthesize complex and longer FAs. To address whether the effects exerted by ACC1 targeting were dependent on the intracellular availability of complex FAs (BCFAs and VLCFAs) whose elongation is malonyl-CoA dependent, we treated LTED cells with TOFA either in the presence or absence of exogenous FA. Adrenic acid (AdA, C22:4; all-cis-7,10,13,16-docosatetraenoic acid), erucic acid (EA, C22:1; cis-13-docosenoic acid), and the BCFA phytanic acid (PHY, C20; 3,7,11,15-tetramethyl hexadecanoic acid) were individually added to LTED cell medium concomitantly to TOFA (Fig. 6A). AdA, EA, and PHY administration completely reverted the decrease in LD content (fig. S6D) and the cell survival inhibitory effect of TOFA (Fig. 6, B to D, and fig. S6E). To exclude that the

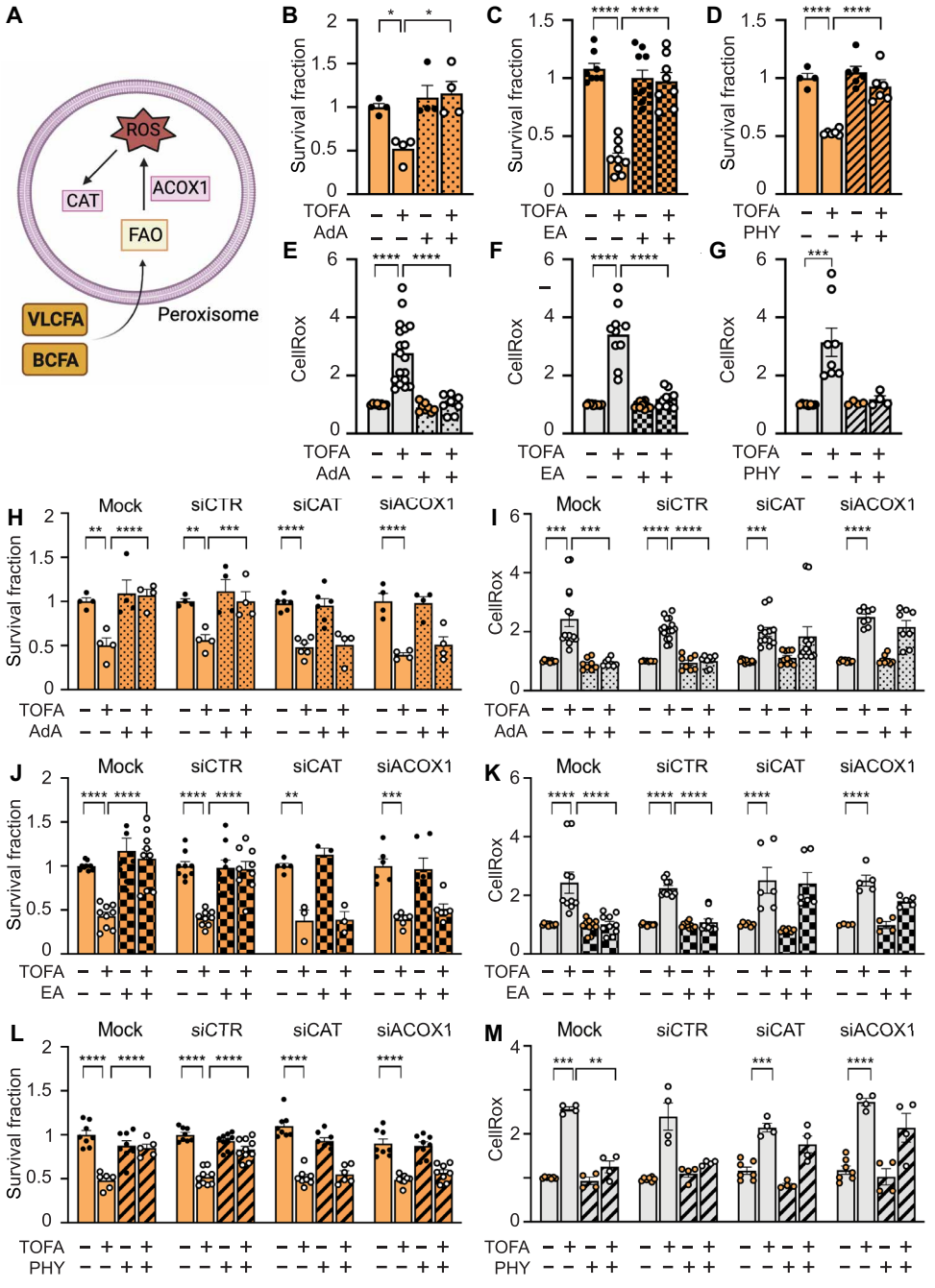

Fig. 6. ACC1 activity is dispensable for LTED cells in the presence of exogenous VLCFAs. (**A**) Schematic of the molecular players involved in peroxisome-dependent FAO and ROS scavenging. (**B** to **G**) MCF7-LTED cells treated with TOFA (0.5 μg/ml) and supplemented with 10 μM VLCFA 22:4 [adrenic acid (AdA), B and E] and 22:1 [erucic acid (EA), C and F] or BCFA [22:0 phytanic acid (PHY), D and G] for 72 hours assayed for (B to D) cell survival and (E to G) ROS using the fluorescent probe CellROX. (B to D) Each dot is a biological replicate. (E to G) $n = 4$ biological replicates. Each dot is a technical replicate. One-way ANOVA, Dunnett-corrected (C to F) or (B and G) Kruskal-Wallis, Dunn-corrected. (**H** to **M**) LTED MCF7 cell derivatives transfected with nontargeting small interfering RNA (siCTR) or siRNA targeting CAT (siCAT) or ACOX1 (siACOX1) and supplemented with 10 μM AdA (H and I), EA (J and K), or PHY (L and M) were assayed for (H, J, and L) cell survival and (I, K, and M) ROS as in (B) to (D). $n = 3$ biological replicates. Each dot is a technical replicate. (H, J, K, and L) Two-way ANOVA, Bonferroni-corrected (I and M), mixed-effects model (REML) Bonferroni-corrected. All data are mean ± SEM. *$P < 0.05$; **$P < 0.01$; ***$P < 0.001$; ****$P < 0.0001$.

effects were independent of FA length, we performed the same assay with palmitic acid (C16:0; hexadecanoic acid) and palmitoleic acid (C16:1; 9Z-hexadecenoic acid) that showed no rescue effect in LTED cells treated with TOFA (fig. S6F). The rescue effect exerted by exogenous FA was accompanied by complete abrogation of the TOFA-induced enhanced ROS (Fig. 6, E to G, and fig. S6G). We therefore hypothesized that VLCFA and BCFA rescue effects could be linked to their ability to coordinate the LTED cellular redox and lipid homeostasis. Because FA catabolism might cause redox unbalance and VLCFA and BCFA catabolism is peroxisome dependent, we investigated whether ACOX1 and CAT silencing affected the exogenous FA rescue effects. Both CAT and ACOX1 silencing (fig. S7, A and B) impeded the ability of AdA (Fig. 6H), EA (Fig. 6J), and PHY (Fig. 6L) to impair the TOFA resensitization effects, a phenomenon that was linked to oxidative stress as shown by enhanced ROS (Fig. 6, I, K, and M). The concomitant inhibition of lipid mobilization from LD and peroxisomal activity also affected LTED cell survival (fig. S7C).

NADPH functions as cofactor of several antioxidant enzymes and has a crucial role in maintaining redox balance. CAT needs NADPH to recharge its antioxidant activity after H_2O_2 buffering (*41*). We found that TOFA-mediated inhibition of peroxisomal activity and FA synthesis promoted an increase in NADPH in LTED cells (fig. S7D). NADPH accumulation could lead to NADPH oxidase (NOX) activation, which could sustain ROS production and promote cell death after TOFA treatment. NOX inhibition mediated by APX115 rescued survival and ROS content in LTED cells (fig. S7, E and F).

Targeting ACC1 ex vivo and in vivo reduces estrogen-independent tumor growth

To validate the above in vitro findings in a clinically relevant model of AI resistance, we monitored FA metabolism–related proteins that were deregulated in the LTED cells in two established ER$^+$ HER2$^-$ breast cancer patient-derived xenograft (PDX) models (HBCx-34 and HBCx-86). These models were made resistant in vivo to estrogen deprivation by ovariectomy (HBCx-34 OvaR and HBCx-86 OvaR), de facto modeling AI resistance (*42*). qRT-PCR (Fig. 7A) and Western blot (Fig. 7B) analyses showed deregulated mRNA and phosphoprotein abundance of key lipid metabolic players in the resistant OvaR PDX models compared with parental HBCx-34 and HBCx-86 PDXs, in line with results in the LTED cells. This suggested a higher lipid metabolic dependency of the resistant PDX. To test whether ACC1 targeting could be exploited in this setting, we first generated ex vivo tumor explants (PDEs) (*43*) from the HBCx-34 and HBCx-86 PDX models and their estrogen-independent (OvaR) counterparts. Three days of TOFA administration reduced HBCx-34 OvaR

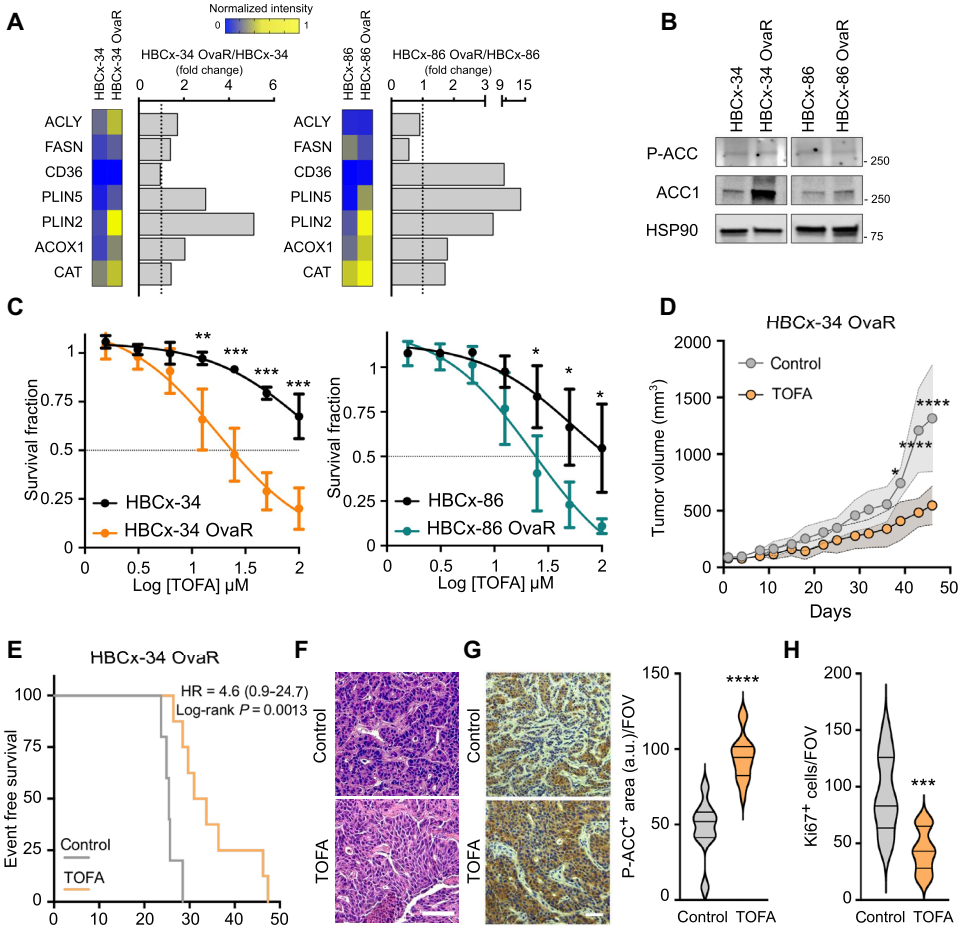

Fig. 7. Targeting ACC1 ex vivo and in vivo reverts resistance to estrogen deprivation. (**A**) Gene expression analysis of sensitive (HBCx-34 and HBCx-86) and estrogen deprivation–resistant PDXs (HBCx34-OvaR and HBCx86-OvaR). Heatmaps show normalized expression values of the mean of three technical replicates, and adjacent bar graphs show fold change expression value relative to the sensitive PDX mean values. (**B**) Western blot analysis of total protein lysate from HBCx and HBCx-OvaR with the antibodies indicated. (**C**) Cell viability of three-dimensional explants derived from HBCx-34 and HBCx-86 and OvaR counterparts and exposed for 72 hours to different concentrations of TOFA. Data are mean ± SEM. $n = 3$ biological replicates. Two-way ANOVA, Bonferroni-corrected. (**D**) In vivo response to TOFA treatment in the HBCx-34 OvaR PDX. Data are mean ± SD. (n = 5 to 8 mice per group). Mixed-effects model (REML) Bonferroni-corrected. (**E**) Survival curves with event-free survival. Median survival control 23.0 and TOFA 33.5. HR and 95% confidence are reported. (**F**) Representative 20× images of hematoxylin and eosin staining. Scale bar, 200 µm. (**G**) Representative 10× images of P-ACC staining and quantification of three different areas derived from at least three samples per group. Violin plots show the distribution, median, and quartile values. Student's t test. Scale bar, 200 µm. (**H**) Quantification of the proliferation index of the PDXs, obtained by quantifying the Ki67-positive cells from three different areas derived at least from three samples per group. Violin plots show the distribution, median, and quartiles values. Student's t test. *$P < 0.05$; **$P < 0.01$; ***$P < 0.001$; ****$P < 0.0001$. a.u., arbitrary units.

and HBCx-86 OvaR PDE survival in a dose-dependent manner, whereas estrogen-dependent PDEs were less sensitive to TOFA administration, a feature shown in an additional PDE derived from the HBCx-91 OvaR model (Fig. 7C and fig. S7G). HBCx-34 OvaR PDX-bearing mice administered TOFA for 46 days showed reduced PDX tumor volume (Fig. 7D) and reduced tumor growth rate (Fig. 7E) compared with vehicle-treated PDX tumors. Moreover, TOFA administration did not appreciably alter tumor morphology, as shown by hematoxylin and eosin staining (Fig. 7F) and showed no toxicity in tumor-bearing mice (fig. S7H). TOFA also inhibited ACC1 activity, as revealed by increased phospho-ACC1 (P-ACC$^+$) immunohistochemistry (IHC) staining (Fig. 7G), and reduced proliferation rate, as confirmed by reduced Ki67 (Fig. 7H). These data provide mechanistic insights into the regulation of lipid metabolism in endocrine-resistant breast cancer and identify peroxisome- and LD-related molecules that could be targeted or investigated as potential predictive markers.

DISCUSSION

Our data demonstrate that the insensitivity to estrogen deprivation, a condition that mimics resistance to AI in ER$^+$ breast cancer, is characterized by a profound rearrangement of lipid metabolism. Previous studies have reported that increased cholesterol biosynthesis is involved in endocrine therapy resistance. Here, we highlighted that LDs and peroxisomes promote deregulation of the FA biosynthesis, storage, and catabolism that drive insensitivity to estrogen deprivation.

Metabolic adaptability is a feature of therapy-resistant cancer cells, including those that are insensitive to endocrine therapy. We have previously demonstrated that deregulated amino acids and central carbon metabolism emerged from preclinical endocrine-resistant models, revealing both targetable metabolic vulnerabilities and key molecular hubs that may have predictive value in the context of therapy resistance (*6*, *7*). More recently, we have shown that targeting oxidative phosphorylation with the complex I inhibitor IACS-010759 potentiates the efficacy of endocrine agents and CDK4/6 inhibitors. Moreover, IACS-010759 inhibits tumor growth in multiple endocrine and palbociclib-resistant PDX models (*44*).

In the current study, we highlighted substantial differences in FA metabolism and subsequent LD formation of LTED cells compared with parental cells. Specifically, we identified ACC1 as a metabolic vulnerability that can be targeted in the context of endocrine resistance.

ACC1 targeting has been shown to reduce tumor initiation capacity in breast cancers (*45*). Moreover, an early study showed that ACC1 is a vulnerability of breast cancer cells in vitro and that its impairment is bypassed when exogenous FA or ROS scavengers are supplemented to the cultured medium (*46*). Although the effects were comparable in ER$^+$ MCF7 and triple-negative MDA-MB-231 breast cancer cells, later studies reported that ER silencing decreases ACC1 expression (*47*), whereas HER2 ectopic expression leads to its increase (*48*) in breast cancer cells. LTED models and the majority of AI-resistant breast cancers retain ER expression (*20*) and overexpress HER2 (*49*), suggesting that increased ACC1 abundance may be a common feature of endocrine-resistant models that retain ER or overexpress HER2. However, ACC1 is tightly regulated by phosphorylation, and its expression may not fully recapitulate its functional role in the disease.

We extensively characterized the role of LDs in the LTED cells and demonstrated that they can release FAs during energetic stress conditions, thus conferring enhanced metabolic flexibility to cells modeling AI resistance. LTED cells maintain the intracellular pool of LDs either by de novo FA biosynthesis or by CD36-mediated VLCFA/BCFA uptake. Increased lipogenesis is a trait of cancer cells (*50*) independent of exogenous FA availability. However, more recently, CD36 emerged as a functional molecule in oral cancer cells that rely on exogenous FA for metastasis formation (*51*). In the context of breast cancer, CD36 expression increases after anti-HER2 therapy and drives therapy desensitization accompanied by metabolic rewiring, ultimately identifying a subset of CD36-higher–expressing patients characterized by poor survival (*52*). Although concomitant CD36-mediated FA upload and de novo lipogenesis could reflect different cell subtypes within the tumor bulk that rely on lipid metabolism, there is emerging evidence that CD36 can directly mediate lipogenesis and LD formation via INSIG2-dependent SREBP1 processing (*53*). At the same time, LTED cells maintain a high dependency on FAO, a similar lipid metabolic program that has been described in residual cancer cells from neoadjuvant-treated patients with breast cancer (*16*). Although LTED cell lipid metabolism was reprogrammed compared with parental cells, only ACC1 targeting selectively reduced LTED cell survival, a condition that was anticipated by intracellular LD reduction. Both in vitro and ex vivo targeting of ACC1 using TOFA reduced survival of cancer cells and estrogen deprivation–resistant PDE models, suggesting the possibility of combining ACC1 targeting with an AI in the resistant setting. However, TOFA administration was not sufficient to completely arrest PDX tumor growth in vivo. Although this could be related to the metabolic plasticity of these resistant tumors or the emergence of resistance to TOFA, a more potent ACC1 inhibitor should be tested. There is an intense effort to develop compounds that can achieve ACC1 inhibition at lower concentrations (*54*, *55*).

Because malonyl-CoA produced by ACC1 is an essential metabolite to generate complex and elongated FAs such as BCFAs and VLCFAs, we hypothesized that ACC1 targeting could be bypassed by the addition of BCFAs and VLCFAs. This approach revealed that BCFA and VLCFA supplementation was sufficient to render ACC1 targeting unsuccessful and that such an effect was mediated by the activity of peroxisome-related enzymes ACOX1 and CAT. These data highlighted that the enhanced peroxisome and LD abundances have a functional role in metabolic plasticity. The data herein presented indicate that peroxisomes have an important function in modulating energy and redox homeostasis when lipogenesis is impaired. No changes in cancer cell survival were observed in normal culture conditions when ACOX1 and CAT were silenced. ACOX1 has prognostic value in ER$^+$ breast cancer, with poorer prognosis in higher expressing tumors (*56*), and ACOX1 is also highly expressed in breast cancer–derived brain metastatic lesions (*57*). Data on CAT expression and function in breast cancer are scarce; however, enhanced CAT expression in MCF7 cells is associated with increased antioxidant activity and therapy resistance (*58*), and targeting CAT in vivo suppresses ROS-driven breast cancer progression and metastasis (*59*). Our findings indicate that peroxisomes may support the metabolic plasticity of endocrine-resistant cells by providing catabolic support when VLCFAs and BCFAs are available. Reducing the amount of free FAs and particularly polyunsaturated fatty acids (PUFAs) is important because PUFAs are highly susceptible to peroxidation, an aspect relevant in cancer cells where ROS are

generally elevated (such as in LTED cells). When abundant, PUFAs are incorporated into the plasma membrane by long-chain acyl-CoA synthetase 4 (ACSL4) and become vulnerable to lipid peroxidation, thus leading to ferroptosis (*60*). Although TOFA did not induce ferroptosis in the LTED models, ACSL4 could have a ferroptosis-independent role during adaptation to estrogen deprivation by channeling BCFAs and VLCFAs into the peroxisome (fig. S7I). Forced expression of ACSL4 confers aggressive traits to breast cancer cells (*61*) and endocrine resistance (*62*).

Intracellular FA homeostasis is maintained by both catabolic and anabolic processes. Peroxisomes not only are important for the catabolism of complex FAs but are also involved in biosynthesis of ether phospholipids, a class of glycerophospholipids that are an essential source of lipid second messengers (arachidonic acid and eicosanoids) and that are involved in PUFA biosynthesis (*63*). LDs can represent the site of eicosanoid production and contribute to generate lipid-derived signaling molecules (*64*). Although this aspect was not investigated in the current study, we cannot exclude that lipid-derived second messengers produced within peroxisomes or derived from LD-peroxisome cross-talk may have a role in breast cancer therapy resistance. Moreover, because peroxisome biogenesis and activity are influenced by three subtypes of peroxisome proliferator–activated receptor (PPAR) transcriptional factors (PPARα, PPARδ, and PPARγ) that are deregulated in several cancers (*65*), PPAR modulators could be investigated in the context of endocrine resistance.

Although interventions to affect metabolic reprogramming have been postulated in the last decades, the compounds approved for therapeutic intervention on metabolic pathways are chemotherapeutic agents that impair nucleic acid synthesis. Because patients who enter clinical trials for innovative drugs are often heavily pretreated (with progressed or relapsed therapy-resistant disease), it is possible that those patients would show enhanced metabolic plasticity, a major challenge when targeting metabolic pathways as demonstrated in our preclinical studies. To circumvent this issue, the highlighted metabolic vulnerabilities that characterized resistant tumors could potentially be targeted using dietary therapies including energy or macronutrient restriction and intermittent fasting regimens. It has been shown that intermittent fasting can potentiate the effects of endocrine agents (*66*), an approach that has been effectively translated into phase 1 clinical trials (NCT03595540 and NCT03340935).

Our study has some limitations and leaves some open questions. First, although TOFA is highly effective in reducing tumor cell growth in vitro, it only slows tumor growth in vivo. Moreover, it has been reported that ACC1 targeting could potentiate the metastatic abilities of breast cancer cells characterized by leptin- and transforming growth factor β–induced downstream signaling activation (*33*). Therefore, ACC1 inhibition should warrant further investigation to identify those breast cancer subtypes that may benefit from this approach. Second, this study did not fully dissect the complex interaction among LDs, mitochondria, and peroxisomes. However, targeting ACOX1 and CAT showed a key role for the peroxisome in the metabolism of complex FA in the LTED models. Moreover, it indicates that complex FAs need to be present in the tumor cells (either by exogenous loading or de novo synthesis). Further, experiments on the FA shuttling among LD, peroxisomes, and mitochondria would shed light on this interaction. Last, ER^+ breast cancer suffers from a lack of syngeneic in vivo models; therefore, it is important to take into consideration that the immune compartment may have a role in therapy response when lipid metabolism is altered by metabolic intervention (*67*).

In conclusion, we identified a complex lipid metabolic reprogramming that characterizes AI resistance and involves multiple intracellular players, including LDs and peroxisomes. These findings provide mechanistic insights into the metabolic deregulation of acquired resistance to estrogen deprivation and offer a series of molecular and metabolic players that could be useful in identifying patients with breast cancer with an increased risk of relapse or therapy resistance.

MATERIALS AND METHODS

Study design

This study consists of a series of preclinical cellular and animal models complemented with human tumor explants, designed to investigate the lipid metabolic rewiring occurring during response and acquisition to estrogen independence in ER^+ breast cancer, a condition that mimics the acquired resistance to AI. Numbers of replicates are explicitly indicated, and all tests of statistical significance are described in the main text, figure captions, or Materials and Methods. For the in vivo experiment, PDXs were randomly assigned to the different treatment groups when tumors reached a volume of 100 to 200 mm^3. The number of animals was chosen to ensure adequate statistical power and was based on previous experience with the PDX models used in this study. Researchers were not blinded for any experiments.

Establishment of PDX mouse models and in vivo experiments

PDX models HBCx-86 and HBCx34 were obtained by engrafting tumor fragments of primary ER^+ breast cancers as previously described (*42*, *68*). The protocol was approved by the Institut Curie Hospital committee (Comité de Revue Institutionnel). Tumor fragments were engrafted with informed consent from the patient into the interscapular fat pads of female Swiss nude mice (Charles River Laboratories), which were maintained under specific pathogen–free conditions. The housing facility was kept at 22°C (±2°C) with a relative humidity of 30 to 70%. The light/dark cycle was 12 hours light/12 hours dark. Mice were maintained on a standard diet (4RF25, Mucedola SRL, Italy) and were given free access to food and water. Animal care and housing were in accordance with institutional guidelines and the rules of the French Ethics Committee CEEA-IC (Comité d'Ethique en matière d'expérimentation animale de l'Institut Curie, national registration number: 118) with project authorization number 02163.02.

In vivo studies were performed in female Swiss nude mice in accordance with the French Ethical Committee. To establish hormone-resistant models from these xenografts, tumor-bearing mice were estrogen-deprived for 6 to 8 months [the absence of estrogen supplementation combined with mice ovariectomy (*42*)]. At tumor escape, tumors were re-engrafted in ovariectomized nude mice in the absence of estrogen supplementation for multiple serial passages.

The in vivo efficacy study with TOFA was performed in female Swiss nude mice as in accordance with the French Ethical Committee. TOFA was administered orally at a dose of 50 mg/kg 5 days/week during 6 weeks. Tumor fragments were transplanted into ovariectomized female 8-week-old Swiss nude mice. Xenografts

were randomly assigned to the different treatment groups when tumors reached a volume between 100 and 200 mm^3. Three mice in the control group unexpectedly died in the first week and were not plotted in the final graph. Tumor size was measured with a manual caliper twice per week. Tumor volume was calculated as $V = a \times b^2/2$, a being the largest diameter and b being the smallest.

Statistical analysis

Statistics were performed using Prism 10 (GraphPad Software). Unless stated otherwise, all numerical data are expressed as the mean ± SEM. All experiments were conducted at least three times independently, with more technical replicates for each experimental condition tested. Normality of data distribution was determined by Shapiro-Wilk or D'Agostino-Pearson omnibus (K2) test. Means of two sample groups were compared by an unpaired two-tailed Student's t test for normally distributed data, whereas Mann-Whitney nonparametric testing was used for non-normally distributed data. For comparisons among multiple groups, one- or two-way analysis of variance (ANOVA) tests for normally distributed data or Kruskal-Wallis test for non-normally distributed data followed by Bonferroni's, Tukey, or Dunnett's post hoc analysis were performed. Tumor growth inhibition was analyzed with a mixed-effects model (REML) followed by Bonferroni's multiple comparisons test. Kaplan-Meier survival curves were calculated as described in (*69*). An event was defined as the time to quadruple the initial tumor volume. Multivariate Cox analyses of the patient cohort were done using Prism 10 and log-rank (Mantel-Cox) test, and log-rank hazard ratio (HR) was calculated. $P < 0.05$ was considered statistically significant.

Supplementary Materials

This PDF file includes:
Materials and Methods
Figs. S1 to S7
References (*70*–*78*)

Other Supplementary Material for this manuscript includes the following:
Data files S1 to S3
MDAR Reproducibility Checklist

REFERENCES AND NOTES

1. H. Pan, R. Gray, J. Braybrooke, C. Davies, C. Taylor, P. McGale, R. Peto, K. I. Pritchard, J. Bergh, M. Dowsett, D. F. Hayes, 20-year risks of breast-cancer recurrence after stopping endocrine therapy at 5 years. *N. Engl. J. Med.* **377**, 1836–1846 (2017).
2. patient-level meta-analysis of the randomised trials, Aromatase inhibitors versus tamoxifen in early breast cancer: Patient-level meta-analysis of the randomised trials. *Lancet* **386**, 1341–1352 (2015).
3. P. A. Francis, O. Pagani, G. F. Fleming, B. A. Walley, M. Colleoni, I. Láng, H. L. Gómez, C. Tondini, E. Ciruelos, H. J. Burstein, H. R. Bonnefoi, M. Bellet, S. Martino, C. E. Geyer, M. P. Goetz, V. Stearns, G. Pinotti, F. Puglisi, S. Spazzapan, M. A. Climent, L. Pavesi, T. Ruhstaller, N. E. Davidson, R. Coleman, M. Debled, S. Buchholz, J. N. Ingle, E. P. Winer, R. Maibach, M. Rabaglio-Poretti, B. Ruepp, A. Di Leo, A. S. Coates, R. D. Gelber, A. Goldhirsch, M. M. Regan, SOFT and TEXT Investigators and the International Breast Cancer Study Group, Tailoring adjuvant endocrine therapy for premenopausal breast cancer. *N. Engl. J. Med.* **379**, 122–137 (2018).
4. Early Breast Cancer Trialists' Collaborative Group (EBCTCG), Aromatase inhibitors versus tamoxifen in premenopausal women with oestrogen receptor-positive early-stage breast cancer treated with ovarian suppression: A patient-level meta-analysis of 7030 women from four randomised trials. *Lancet Oncol.* **23**, 382–392 (2022).
5. A. B. Hanker, D. R. Sudhan, C. L. Arteaga, Overcoming endocrine resistance in breast cancer. *Cancer Cell* **37**, 496–513 (2020).
6. M. Bacci, E. Giannoni, A. Fearns, R. Ribas, Q. Gao, M. L. Taddei, G. Pintus, M. Dowsett, C. M. Isacke, L. A. Martin, P. Chiarugi, A. Morandi, miR-155 drives metabolic reprogramming of ER+ breast cancer cells following long-term estrogen deprivation and predicts clinical response to aromatase inhibitors. *Cancer Res.* **76**, 1615–1626 (2016).
7. M. Bacci, N. Lorito, L. Ippolito, M. Ramazzotti, S. Luti, S. Romagnoli, M. Parri, F. Bianchini, F. Cappellesso, F. Virga, Q. Gao, B. M. Simões, E. Marangoni, L. A. Martin, G. Comito, M. Ferracin, E. Giannoni, M. Mazzone, P. Chiarugi, A. Morandi, Reprogramming of amino acid transporters to support aspartate and glutamate dependency sustains endocrine resistance in breast cancer. *Cell Rep.* **28**, 104–118.e8 (2019).
8. T. Du, M. J. Sikora, K. M. Levine, N. Tasdemir, R. B. Riggins, S. G. Wendell, B. Van Houten, S. Oesterreich, Key regulators of lipid metabolism drive endocrine resistance in invasive lobular breast cancer. *Breast Cancer Res.* **20**, 106 (2018).
9. V. T. Nguyen, I. Barozzi, M. Faronato, Y. Lombardo, J. H. Steel, N. Patel, P. Darbre, L. Castellano, B. Győrffy, L. Woodley, A. Meira, D. K. Patten, V. Vircillo, M. Periyasamy, S. Ali, G. Frige, S. Minucci, R. C. Coombes, L. Magnani, Differential epigenetic reprogramming in response to specific endocrine therapies promotes cholesterol biosynthesis and cellular invasion. *Nat. Commun.* **6**, 10044 (2015).
10. Y. Perone, A. J. Farrugia, A. Rodríguez-Meira, B. Győrffy, C. Ion, A. Uggetti, A. Chronopoulos, P. Marrazzo, M. Faronato, S. Shousha, C. Davies, J. H. Steel, N. Patel, A. Del Rio Hernandez, C. Coombes, G. Pruneri, A. Lim, F. Calvo, L. Magnani, SREBP1 drives Keratin-80-dependent cytoskeletal changes and invasive behavior in endocrine-resistant ERα breast cancer. *Nat. Commun.* **10**, 2115 (2019).
11. M. Bacci, N. Lorito, A. Smiriglia, A. Morandi, Fat and furious: Lipid metabolism in antitumoral therapy response and resistance. *Trends Cancer* **7**, 198–213 (2021).
12. S. J. Wakil, L. A. Abu-Elheiga, Fatty acid metabolism: Target for metabolic syndrome. *J. Lipid Res.* **50** Suppl, S138–S143 (2009).
13. J. A. Olzmann, P. Carvalho, Dynamics and functions of lipid droplets. *Nat. Rev. Mol. Cell Biol.* **20**, 137–155 (2019).
14. A. L. S. Cruz, E. A. Barreto, N. P. B. Fazolini, J. P. B. Viola, P. T. Bozza, Lipid droplets: Platforms with multiple functions in cancer hallmarks. *Cell Death Dis.* **11**, 105 (2020).
15. L. Ippolito, G. Comito, M. Parri, M. Iozzo, A. Duatti, F. Virgilio, N. Lorito, M. Bacci, E. Pardella, G. Sandrini, F. Bianchini, R. Damiano, L. Ferrone, G. la Marca, S. Serni, P. Spatafora, C. V. Catapano, A. Morandi, E. Giannoni, P. Chiarugi, Lactate Rewires Lipid Metabolism and Sustains a Metabolic-Epigenetic Axis in Prostate Cancer. *Cancer Res.* **82**, 1267–1282 (2022).
16. K. M. Havas, V. Milchevskaya, K. Radic, A. Alladin, E. Kafkia, M. Garcia, J. Stolte, B. Klaus, N. Rotmensz, T. J. Gibson, B. Burwinkel, A. Schneeweiss, G. Pruneri, K. R. Patil, R. Sotillo, M. Jechlinger, Metabolic shifts in residual breast cancer drive tumor recurrence. *J. Clin. Invest.* **127**, 2091–2105 (2017).
17. M. F. Renne, H. Hariri, Lipid droplet-organelle contact sites as hubs for fatty acid metabolism, trafficking, and metabolic channeling. *Front. Cell Dev. Biol.* **9**, 726261 (2021).
18. L. Ding, W. Sun, M. Balaz, A. He, M. Klug, S. Wieland, R. Caiazzo, V. Raverdy, F. Pattou, P. Lefebvre, I. J. Lodhi, B. Staels, M. Heim, C. Wolfrum, Peroxisomal β-oxidation acts as a sensor for intracellular fatty acids and regulates lipolysis. *Nat. Metab.* **3**, 1648–1661 (2021).
19. J. A. Kim, Peroxisome Metabolism in Cancer. *Cells* **9**, 1692 (2020).
20. A. Morandi, L. A. Martin, Q. Gao, S. Pancholi, A. Mackay, D. Robertson, M. Zvelebil, M. Dowsett, I. Plaza-Menacho, C. M. Isacke, GDNF-RET signaling in ER-positive breast cancers is a key determinant of response and resistance to aromatase inhibitors. *Cancer Res.* **73**, 3783–3795 (2013).
21. A. Cattaneo, G. Martano, U. Restuccia, L. Tronci, M. Bianchi, A. Bachi, V. Matafora, Opti-nQL: An optimized, versatile and sensitive nano-LC method for MS-based lipidomics analysis. *Metabolites* **11**, 720 (2021).
22. W. J. Lin, P. C. Shen, H. C. Liu, Y. C. Cho, M. K. Hsu, I. C. Lin, F. H. Chen, J. C. Yang, W. L. Ma, W. C. Cheng, LipidSig: A web-based tool for lipidomic data analysis. *Nucleic Acids Res.* **49**, W336–W345 (2021).
23. M. R. Molenaar, A. Jeucken, T. A. Wassenaar, C. H. A. van de Lest, J. F. Brouwers, J. B. Helms, LION/web: A web-based ontology enrichment tool for lipidomic data analysis. *Gigascience* **8**, giz061 (2019).
24. V. Brovkovych, A. Aldrich, N. Li, G. E. Atilla-Gokcumen, J. Frasor, Removal of serum lipids and lipid-derived metabolites to investigate breast cancer cell biology. *Proteomics* **19**, e1800370 (2019).
25. P. Khongthong, A. K. Roseweir, J. Edwards, The NF-KB pathway and endocrine therapy resistance in breast cancer. *Endocr. Relat. Cancer* **26**, R369–R380 (2019).
26. D. Capece, D. D'Andrea, F. Begalli, L. Goracci, L. Tornatore, J. L. Alexander, A. Di Veroli, S. C. Leow, T. S. Vaiyapuri, J. K. Ellis, D. Verzella, J. Bennett, L. Savino, Y. Ma, J. S. McKenzie, M. L. Doria, S. E. Mason, K. R. Chng, H. C. Keun, G. Frost, V. Tergaonkar, K. Broniowska, W. Stunkel, Z. Takats, J. M. Kinross, G. Cruciani, G. Franzoso, Enhanced triacylglycerol catabolism by carboxylesterase 1 promotes aggressive colorectal carcinoma. *J. Clin. Invest.* **131**, e137845 (2021).
27. W. M. Henne, M. L. Reese, J. M. Goodman, The assembly of lipid droplets and their roles in challenged cells. *EMBO J.* **37**, e98947 (2018).
28. E. Jarc, T. Petan, Lipid droplets and the management of cellular stress. *Yale J. Biol. Med.* **92**, 435–452 (2019).
29. J. I. López-Velazco, S. Manzano, M. Otaño, K. Elorriaga, N. Bultó, J. Herrero, A. Lahuerta, V. Segur, I. Álvarez-López, M. M. Caffarel, A. Urruticoechea, A prospective study on tumour response assessment methods after neoadjuvant endocrine therapy in early oestrogen receptor-positive breast cancer. *Breast Cancer Res.* **26**, 3 (2024).

30. M. J. Ellis, Y. Tao, J. Luo, R. A'Hern, D. B. Evans, A. S. Bhatnagar, H. A. Chaudri Ross, A. von Kameke, W. R. Miller, I. Smith, W. Eiermann, M. Dowsett, Outcome prediction for estrogen receptor-positive breast cancer based on postneoadjuvant endocrine therapy tumor characteristics. *J. Natl. Cancer Inst.* **100**, 1380–1388 (2008).
31. M. J. Ellis, V. J. Suman, J. Hoog, R. Goncalves, S. Sanati, C. J. Creighton, K. DeSchryver, E. Crouch, A. Brink, M. Watson, J. Luo, Y. Tao, M. Barnes, M. Dowsett, G. T. Budd, E. Winer, P. Silverman, L. Esserman, L. Carey, C. X. Ma, G. Unzeitig, T. Pluard, P. Whitworth, G. Babiera, J. M. Guenther, Z. Dayao, D. Ota, M. Leitch, J. A. Olson, D. C. Allred, K. Hunt, Ki67 proliferation index as a tool for chemotherapy decisions during and after neoadjuvant aromatase inhibitor treatment of breast cancer: Results from the American college of surgeons oncology group Z1031 trial (Alliance). *J. Clin. Oncol.* **35**, 1061–1069 (2017).
32. R. U. Svensson, S. J. Parker, L. J. Eichner, M. J. Kolar, M. Wallace, S. N. Brun, P. S. Lombardo, J. L. Van Nostrand, A. Hutchins, L. Vera, L. Gerken, J. Greenwood, S. Bhat, G. Harriman, W. F. Westlin, H. J. Harwood, A. Saghatelian, R. Kapeller, C. M. Metallo, R. J. Shaw, Inhibition of acetyl-CoA carboxylase suppresses fatty acid synthesis and tumor growth of non-small-cell lung cancer in preclinical models. *Nat. Med.* **22**, 1108–1119 (2016).
33. M. Rios Garcia, B. Steinbauer, K. Srivastava, M. Singhal, F. Mattijssen, A. Maida, S. Christian, H. Hess-Stumpp, H. G. Augustin, K. Müller-Decker, P. P. Nawroth, S. Herzig, M. Berriel Diaz, Acetyl-CoA Carboxylase 1-dependent protein acetylation controls breast cancer metastasis and recurrence. *Cell Metab.* **26**, 842–855.e5 (2017).
34. A. P. Bailey, G. Koster, C. Guillermier, E. M. Hirst, J. I. MacRae, C. P. Lechene, A. D. Postle, A. P. Gould, Antioxidant role for lipid droplets in a stem cell niche of drosophila. *Cell* **163**, 340–353 (2015).
35. W. S. Yang, B. R. Stockwell, Ferroptosis: Death by lipid peroxidation. *Trends Cell Biol.* **26**, 165–176 (2016).
36. R. J. Wanders, Metabolic functions of peroxisomes in health and disease. *Biochimie* **98**, 36–44 (2014).
37. B. Pereira, S. F. Chin, O. M. Rueda, H. K. Vollan, E. Provenzano, H. A. Bardwell, M. Pugh, L. Jones, R. Russell, S. J. Sammut, D. W. Tsui, B. Liu, S. J. Dawson, J. Abraham, H. Northen, J. F. Peden, A. Mukherjee, G. Turashvili, A. R. Green, S. McKinney, A. Oloumi, S. Shah, N. Rosenfeld, L. Murphy, D. R. Bentley, I. O. Ellis, A. Purushotham, S. E. Pinder, A. L. Børresen-Dale, H. M. Earl, P. D. Pharoah, M. T. Ross, S. Aparicio, C. Caldas, The somatic mutation profiles of 2,433 breast cancers refines their genomic and transcriptomic landscapes. *Nat. Commun.* **7**, 11479 (2016).
38. H. Kennecke, R. Yerushalmi, R. Woods, M. C. Cheang, D. Voduc, C. H. Speers, T. O. Nielsen, K. Gelmon, Metastatic behavior of breast cancer subtypes. *J. Clin. Oncol.* **28**, 3271–3277 (2010).
39. W. R. Miller, A. A. Larionov, L. Renshaw, T. J. Anderson, S. White, J. Murray, E. Murray, G. Hampton, J. R. Walker, S. Ho, A. Krause, D. B. Evans, J. M. Dixon, Changes in breast cancer transcriptional profiles after treatment with the aromatase inhibitor, letrozole. *Pharmacogenet. Genomics* **17**, 813–826 (2007).
40. T. Sassa, A. Kihara, Metabolism of very long-chain Fatty acids: Genes and pathophysiology. *Biomol. Ther. (Seoul)* **22**, 83–92 (2014).
41. H. N. Kirkman, G. F. Gaetani, Catalase: A tetrameric enzyme with four tightly bound molecules of NADPH. *Proc. Natl. Acad. Sci. U.S.A.* **81**, 4343–4347 (1984).
42. P. Cottu, I. Bièche, F. Assayag, R. El Botty, S. Chateau-Joubert, A. Thuleau, T. Bagarre, B. Albaud, A. Rapinat, D. Gentien, P. de la Grange, V. Sibut, S. Vacher, R. Hatem, J. L. Servely, J. J. Fontaine, D. Decaudin, J. Y. Pierga, S. Roman-Roman, E. Marangoni, Acquired resistance to endocrine treatments is associated with tumor-specific molecular changes in patient-derived luminal breast cancer xenografts. *Clin. Cancer Res.* **20**, 4314–4325 (2014).
43. A. Bruna, O. M. Rueda, W. Greenwood, A. S. Batra, M. Callari, R. N. Batra, K. Pogrebniak, J. Sandoval, J. W. Cassidy, A. Tufegdzic-Vidakovic, S. J. Sammut, L. Jones, E. Provenzano, R. Baird, P. Eirew, J. Hadfield, M. Eldridge, A. McLaren-Douglas, A. Barthorpe, H. Lightfoot, M. J. O'Connor, J. Gray, J. Cortes, J. Baselga, E. Marangoni, A. L. Welm, S. Aparicio, V. Serra, M. J. Garnett, C. Caldas, A biobank of breast cancer explants with preserved intra-tumor heterogeneity to screen anticancer compounds. *Cell* **167**, 260–274.e22 (2016).
44. R. El-Botty, L. Morriset, E. Montaudon, Z. Tariq, A. Schnitzler, M. Bacci, N. Lorito, L. Sourd, L. Huguet, A. Dahmani, P. Painsec, H. Derrien, S. Vacher, J. Masliah-Planchon, V. Raynal, S. Baulande, T. Larcher, A. Vincent-Salomon, G. Dutertre, P. Cottu, G. Gentric, F. Mechta-Grigoriou, S. Hutton, K. Driouch, I. Bièche, A. Morandi, E. Marangoni, Oxidative phosphorylation is a metabolic vulnerability of endocrine therapy and palbociclib resistant metastatic breast cancers. *Nat. Commun.* **14**, 4221 (2023).
45. B. Corominas-Faja, E. Cuyàs, J. Gumuzio, J. Bosch-Barrera, O. Leis, Á. Martin, J. A. Menendez, Chemical inhibition of acetyl-CoA carboxylase suppresses self-renewal growth of cancer stem cells. *Oncotarget* **5**, 8306–8316 (2014).
46. V. Chajès, M. Cambot, K. Moreau, G. M. Lenoir, V. Joulin, Acetyl-CoA carboxylase alpha is essential to breast cancer cell survival. *Cancer Res.* **66**, 5287–5294 (2006).
47. M. E. Monaco, Fatty acid metabolism in breast cancer subtypes. *Oncotarget* **8**, 29487–29500 (2017).
48. S. Yoon, M. Y. Lee, S. W. Park, J. S. Moon, Y. K. Koh, Y. H. Ahn, B. W. Park, K. S. Kim, Up-regulation of acetyl-CoA carboxylase alpha and fatty acid synthase by human epidermal growth factor receptor 2 at the translational level in breast cancer cells. *J. Biol. Chem.* **282**, 26122–26131 (2007).
49. L. A. Martin, I. Farmer, S. R. Johnston, S. Ali, C. Marshall, M. Dowsett, Enhanced estrogen receptor (ER) alpha, ERBB2, and MAPK signal transduction pathways operate during the adaptation of MCF-7 cells to long term estrogen deprivation. *J. Biol. Chem.* **278**, 30458–30468 (2003).
50. J. A. Menendez, R. Lupu, Fatty acid synthase and the lipogenic phenotype in cancer pathogenesis. *Nat. Rev. Cancer* **7**, 763–777 (2007).
51. G. Pascual, A. Avgustinova, S. Mejetta, M. Martín, A. Castellanos, C. S. Attolini, A. Berenguer, N. Prats, A. Toll, J. A. Hueto, C. Bescós, L. Di Croce, S. A. Benitah, Targeting metastasis-initiating cells through the fatty acid receptor CD36. *Nature* **541**, 41–45 (2017).
52. W. W. Feng, O. Wilkins, S. Bang, M. Ung, J. Li, J. An, C. Del Genio, K. Canfield, J. DiRenzo, W. Wells, A. Gaur, R. B. Robey, J. Y. Guo, R. L. Powles, C. Sotiriou, L. Pusztai, M. Febbraio, C. Cheng, W. B. Kinlaw, M. Kurokawa, CD36-mediated metabolic rewiring of breast cancer cells promotes resistance to HER2-targeted therapies. *Cell Rep.* **29**, 3405–3420.e5 (2019).
53. H. Zeng, H. Qin, M. Liao, E. Zheng, X. Luo, A. Xiao, Y. Li, L. Chen, L. Wei, L. Zhao, X. Z. Ruan, P. Yang, Y. Chen, CD36 promotes de novo lipogenesis in hepatocytes through INSIG2-dependent SREBP1 processing. *Mol. Metab.* **57**, 101428 (2022).
54. B. Batchuluun, S. L. Pinkosky, G. R. Steinberg, Lipogenesis inhibitors: Therapeutic opportunities and challenges. *Nat. Rev. Drug Discov.* **21**, 283–305 (2022).
55. R. Mizojiri, D. Tomita, M. Sasaki, Y. Satoh, Y. Yamamoto, H. Sumi, H. Maezaki, Design and synthesis of a monocyclic derivative as a selective ACC1 inhibitor by chemical modification of biphenyl ACC1/2 dual inhibitors. *Bioorg. Med. Chem.* **35**, 116056 (2021).
56. S. Kim, Y. Lee, J. S. Koo, Differential expression of lipid metabolism-related proteins in different breast cancer subtypes. *PLoS One* **10**, e0119473 (2015).
57. Y. Y. Jung, H. M. Kim, J. S. Koo, Expression of lipid metabolism-related proteins in metastatic breast cancer. *PLoS One* **10**, e0137204 (2015).
58. C. Glorieux, J. Auquier, N. Dejeans, B. Sid, J. B. Demoulin, L. Bertrand, J. Verrax, P. B. Calderon, Catalase expression in MCF-7 breast cancer cells is mainly controlled by PI3K/Akt/mTor signaling pathway. *Biochem. Pharmacol.* **89**, 217–223 (2014).
59. J. Goh, L. Enns, S. Fatemie, H. Hopkins, J. Morton, C. Pettan-Brewer, W. Ladiges, Mitochondrial targeted catalase suppresses invasive breast cancer in mice. *BMC Cancer* **11**, 191 (2011).
60. S. Doll, B. Proneth, Y. Y. Tyurina, E. Panzilius, S. Kobayashi, I. Ingold, M. Irmler, J. Beckers, M. Aichler, A. Walch, H. Prokisch, D. Trümbach, G. Mao, F. Qu, H. Bayir, J. Füllekrug, C. H. Scheel, W. Wurst, J. A. Schick, V. E. Kagan, J. P. Angeli, M. Conrad, ACSL4 dictates ferroptosis sensitivity by shaping cellular lipid composition. *Nat. Chem. Biol.* **13**, 91–98 (2017).
61. X. Wu, Y. Li, J. Wang, X. Wen, M. T. Marcus, G. Daniels, D. Y. Zhang, F. Ye, L. H. Wang, X. Du, S. Adams, B. Singh, J. Zavadil, P. Lee, M. E. Monaco, Long chain fatty Acyl-CoA synthetase 4 is a biomarker for and mediator of hormone resistance in human breast cancer. *PLoS One* **8**, e77060 (2013).
62. U. D. Orlando, A. F. Castillo, M. A. R. Medrano, A. R. Solano, P. M. Maloberti, E. J. Podesta, Acyl-CoA synthetase-4 is implicated in drug resistance in breast cancer cell lines involving the regulation of energy-dependent transporter expression. *Biochem. Pharmacol.* **159**, 52–63 (2019).
63. M. C. F. Messias, G. C. Mecatti, D. G. Priolli, P. de Oliveira Carvalho, Plasmalogen lipids: Functional mechanism and their involvement in gastrointestinal cancer. *Lipids Health Dis.* **17**, 41 (2018).
64. P. T. Bozza, I. Bakker-Abreu, R. A. Navarro-Xavier, C. Bandeira-Melo, Lipid body function in eicosanoid synthesis: An update. *Prostaglandins Leukot. Essent. Fatty Acids* **85**, 205–213 (2011).
65. L. Michalik, B. Desvergne, W. Wahli, Peroxisome-proliferator-activated receptors and cancers: Complex stories. *Nat. Rev. Cancer* **4**, 61–70 (2004).
66. I. Caffa, V. Spagnolo, C. Vernieri, F. Valdemarin, P. Becherini, M. Wei, S. Brandhorst, C. Zucal, E. Driehuis, L. Ferrando, F. Piacente, A. Tagliafico, M. Cilli, L. Mastracci, V. G. Vellone, S. Piazza, A. L. Cremonini, R. Gradaschi, C. Mantero, M. Passalacqua, A. Ballestrero, G. Zoppoli, M. Cea, A. Arrighi, P. Odetti, F. Monacelli, G. Salvadori, S. Cortellino, H. Clevers, F. De Braud, S. G. Sukkar, A. Provenzani, V. D. Longo, A. Nencioni, Fasting-mimicking diet and hormone therapy induce breast cancer regression. *Nature* **583**, 620–624 (2020).
67. H. Prendeville, L. Lynch, Diet, lipids, and antitumor immunity. *Cell. Mol. Immunol.* **19**, 432–444 (2022).
68. E. Marangoni, A. Vincent-Salomon, N. Auger, A. Degeorges, F. Assayag, P. de Cremoux, L. de Plater, C. Guyader, G. De Pinieux, J. G. Judde, M. Rebucci, C. Tran-Perennou, X. Sastre-Garau, B. Sigal-Zafrani, O. Delattre, V. Diéras, M. F. Poupon, A new model of patient tumor-derived breast cancer xenografts for preclinical assays. *Clin. Cancer Res.* **13**, 3989–3998 (2007).
69. P. J. Houghton, C. L. Morton, C. Tucker, D. Payne, E. Favours, C. Cole, R. Gorlick, E. A. Kolb, W. Zhang, R. Lock, H. Carol, M. Tajbakhsh, C. P. Reynolds, J. M. Maris, J. Courtright, S. T. Keir, H. S. Friedman, C. Stopford, J. Zeidner, J. Wu, T. Liu, C. A. Billups, J. Khan, S. Ansher, J. Zhang, M. A. Smith, The pediatric preclinical testing program: Description of models and early testing results. *Pediatr. Blood Cancer* **49**, 928–940 (2007).
70. F. Ye, C. L. Hoppel, Measuring oxidative phosphorylation in human skin fibroblasts. *Anal. Biochem.* **437**, 52–58 (2013).

71. D. Pesta, E. Gnaiger, High-resolution respirometry: OXPHOS protocols for human cells and permeabilized fibers from small biopsies of human muscle. *Methods Mol. Biol.* **810**, 25–58 (2012).
72. V. J. Suman, M. J. Ellis, C. X. Ma, The ALTERNATE trial: Assessing a biomarker driven strategy for the treatment of post-menopausal women with ER+/Her2- invasive breast cancer. *Chin. Clin. Oncol.* **4**, 34 (2015).
73. T. Wu, E. Hu, S. Xu, M. Chen, P. Guo, Z. Dai, T. Feng, L. Zhou, W. Tang, L. Zhan, X. Fu, S. Liu, X. Bo, G. Yu, clusterProfiler 4.0: A universal enrichment tool for interpreting omics data. *Innovation (Camb)* **2**, 100141 (2021).
74. C. Curtis, S. P. Shah, S. F. Chin, G. Turashvili, O. M. Rueda, M. J. Dunning, D. Speed, A. G. Lynch, S. Samarajiwa, Y. Yuan, S. Gräf, G. Ha, G. Haffari, A. Bashashati, R. Russell, S. McKinney, A. Langerød, A. Green, E. Provenzano, G. Wishart, S. Pinder, P. Watson, F. Markowetz, L. Murphy, I. Ellis, A. Purushotham, A. L. Børresen-Dale, J. D. Brenton, S. Tavaré, C. Caldas, S. Aparicio, METABRIC Group, The genomic and transcriptomic architecture of 2,000 breast tumours reveals novel subgroups. *Nature* **486**, 346–352 (2012).
75. E. Cerami, J. Gao, U. Dogrusoz, B. E. Gross, S. O. Sumer, B. A. Aksoy, A. Jacobsen, C. J. Byrne, M. L. Heuer, E. Larsson, Y. Antipin, B. Reva, A. P. Goldberg, C. Sander, N. Schultz, The cBio cancer genomics portal: An open platform for exploring multidimensional cancer genomics data. *Cancer Discov.* **2**, 401–404 (2012).
76. J. Gao, B. A. Aksoy, U. Dogrusoz, G. Dresdner, B. Gross, S. O. Sumer, Y. Sun, A. Jacobsen, R. Sinha, E. Larsson, E. Cerami, C. Sander, N. Schultz, Integrative analysis of complex cancer genomics and clinical profiles using the cBioPortal. *Sci. Signal.* **6**, pl1 (2013).
77. Cancer Genome Atlas Network, Comprehensive molecular portraits of human breast tumours. *Nature* **490**, 61–70 (2012).
78. W. R. Miller, A. Larionov, Changes in expression of oestrogen regulated and proliferation genes with neoadjuvant treatment highlight heterogeneity of clinical resistance to the aromatase inhibitor, letrozole. *Breast Cancer Res.* **12**, R52 (2010).

Acknowledgments: We thank A. Duatti and A. Guida, who discussed this study and helped with cell culturing during their MSc internship. We thank M. Ramazzotti and D. Capece for critical discussion. **Funding:** The work was funded by Associazione Italiana Ricerca sul Cancro (AIRC) and Fondazione Cassa di Risparmio di Firenze (grant Multiuser 19515 to P.C. and A.M.) and AIRC (grant IG 22941 to A.M. and grant IG 8797 to P.C.), PNRR M4C2-Investimento 1.4-CN00000041 CN3 "Sviluppo di Terapia Genica e Farmaci con Tecnologia ad RNA" funded by NextGenerationEU (to M.C., E.G., and A.M.), PNRR "THE - Tuscany Health Ecosystem" ambito di intervento "1. Health" ECS00000017 funded by NextGenerationEU (to M.B., P.C., and A.M). M.B. was supported by Fondazione Pezcoller/SIC Prof.ssa De Gasperi Ronc. N.L. was supported by an AIRC fellowship. We thank Associazione Annastaccatolisa ODV nonprofit organization for supporting A. Subbiani's fellowship. We extend our thanks to Fondazione Radioterapia Oncologica (FRO) nonprofit organization and all those who have provided essential support for scientific research. Data presented in the current study were in part generated using the equipment of the Facility di Medicina Molecolare, funded by "Ministero dell'Istruzione dell'Università e della Ricerca–Bando Dipartimenti di Eccellenza 2018-2022." Construction of the TMA and analysis of the clinical samples used in this study were funded by Instituto de Salud Carlos III (ISCIII) grant PI20/01253, cofunded by the European Union, Basque Department of Health grant (2020111040), Fundación SEOM (SEOM Avon Fellowship 2020), and AECC PhD Fellowship (PRDGI19007LOPE). Illustrations were created with BioRender.com.
Author contributions: M.B. and N.L. performed cell-based and biochemistry experiments, study design, data acquisition, analysis, and interpretation and revised the original manuscript draft; A. Smiriglia, A. Subbiani, and F.B. performed cell-based and biochemistry experiments and participated in data interpretation; G.C. designed and performed IHC analysis; L.M. and R.E.B. performed the ex vivo and in vivo PDX experiments; M.B. and L.M. performed and interpreted in silico analysis; M.C., L.I., and E.G. developed methodology, provided administrative and technical support, and interpreted data; J.I.L-V., A.U., and M.M.C. generated the TMA and supported IHC analysis; G.S. developed methodology, provided technical support, and interpreted data; I.M. performed data analysis and interpretation and revised the manuscript; V.M., K.H., and A.B. designed and performed LC-MS analysis and data interpretation; P.C. performed data analysis and interpretation and revised the manuscript; E.M. generated PDX models, designed and supervised PDX experiments, performed data analysis and interpretation, and revised the manuscript; A.M. conceived, designed, and supervised the study; performed cell-based and metabolic experiments; analyzed and interpreted data; and wrote the original manuscript draft. All authors reviewed the prepared manuscript. **Competing interests:** I.M. declares consultant honoraria for Eli Lilly, Novartis, Seagen, Istituto Gentili, Roche, Pfizer, Ipsen, and Pierre Fabre. M.B. declares consultant honoraria for Novartis; L.M. reports receiving research grants (institution) from Novartis and Pfizer and consultant honoraria for Novartis, Seagen, and Pfizer. All other authors declare that they have no competing interests. **Data and materials availability:** All data associated with this study are present in the paper or the Supplementary Materials. Raw figure data are in data file S3.

Submitted 24 November 2022
Resubmitted 6 September 2023
Accepted 30 January 2024
Published 28 February 2024
10.1126/scitranslmed.adf9874